The 16th Data Release of the Sloan Digital Sky Surveys

Ahumada, Romina; Prieto, Carlos Allende; Almeida, Andres; Anders, Friedrich; Anderson, Scott F.; Andrews, Brett H.; Anguiano, Borja; Arcodia, Riccardo; Armengaud, Eric; Aubert, Marie; Avila, Santiago; Avila-Reese, Vladimir; Badenes, Carles; Balland, Christophe; Barger, Kat; Barrera-Ballesteros, Jorge K.; Basu, Sarbani; Bautista, Julian; Beaton, Rachael L.; Beers, Timothy C.

DOI:
10.3847/1538-4365/ab929e

Document Version
Publisher's PDF, also known as Version of record

Citation for published version (Harvard):
Ahumada, R, Prieto, CA, Almeida, A, Anders, F, Anderson, SF, Andrews, BH, Anguiano, B, Arcodia, R, Armengaud, E, Aubert, M, Avila, S, Avila-Reese, V, Badenes, C, Balland, C, Barger, K, Barrera-Ballesteros, JK, Basu, S, Bautista, J, Beaton, RL, Beers, TC, Benavides, BIT, Bender, CF, Bernardi, M, Bershady, M, Beutler, F, Bidin, CM, Bird, J, Bizyaev, D, Blanc, GA, Blanton, MR, Boquien, M, Borissova, J, Bovy, J, Brandt, WN, Brinkmann, J, Brownstein, JR, Bundy, K, Bureau, M, Burgasser, A, Burtin, E, Cano-Diaz, M, Capasso, R, Cappellari, M, Carrera, R, Chabanier, S, Chaplin, W, Chapman, M, Cherinka, B, Chiappini, C, Choi, PD, Chojnowski, SD, Chung, H, Clerc, N, Coffey, D, Comerford, JM, Comparat, J, Costa, LD, Cousinou, M-C, Covey, K, Crane, JD, Cunha, K, Ilha, GDS, Dai, YS, Damsted, SB, Darling, J, Jr, JWD, Davies, R, Dawson, K, De, N, Macorra, ADL, Lee, ND, Queiroz, ABDA, Machado, AD, Torre, SDL, Dell'Agli, F, Bourboux, HDMD, Diamond-Stanic, AM, Dillon, S, Donor, J, Drory, N, Duckworth, C, Dwelly, T, Ebelke, G, Eftekharzadeh, S, Eigenbrot, AD, Elsworth, YP, Eracleous, M, Erfanianfar, G, Escoffier, S, Fan, X, Farr, E, Fernandez-Trincado, JG, Feuillet, D, Finoguenov, A, Fofie, P, Fraser-McKelvie, A, Frinchaboy, PM, Fromenteau, S, Fu, H, Galbany, L, Garcia, RA, Garcia-Hernandez, DA, Oehmichen, LAG, Ge, J, Maia, MAG, Geisler, D, Gelfand, J, Goddy, J, Goff, J-ML, Gonzalez-Perez, V, Grabowski, K, Green, P, Grier, CJ, Guo, H, Guy, J, Harding, P, Hasselquist, S, Hawken, AJ, Hayes, CR, Hearty, F, Hekker, S, Hogg, DW, Holtzman, J, Horta, D, Hou, J, Hsieh, B-C, Huber, D, Hunt, JAS, Chitham, JI, Imig, J, Jaber, M, Angel, CEJ, Johnson, JA, Jones, AM, Jonsson, H, Jullo, E, Kim, Y, Kinemuchi, K, Charles, CKIV, Kite, GW, Klaene, M, Kneib, J-P, Kollmeier, JA, Kong, H, Kounkel, M, Krishnarao, D, Lacerna, I, Lan, T-W, Lane, RR, Law, DR, Leung, HW, Lewis, H, Li, C, Lian, J, Lin, L, Long, D, Longa-Pena, P, Lundgren, B, Lyke, BW, Mackereth, JT, MacLeod, CL, Majewski, SR, Manchado, A, Maraston, C, Martini, P, Masseron, T, Masters, KL, Mathur, S, McDermid, RM, Merloni, A, Merrifield, M, Meszaros, S, Miglio, A, Minniti, D, Minsley, R, Miyaji, T, Mohammad, FG, Mosser, B, Mueller, E-M, Muna, D, Munoz-Gutierrez, A, Myers, AD, Nadathur, S, Nair, P, Nandra, K, Nascimento, JCD, Nevin, RJ, Newman, JA, Nidever, DL, Nitschelm, C, Noterdaeme, P, O'Connell, JE, Olmstead, MD, Oravetz, D, Oravetz, A, Osorio, Y, Pace, ZJ, Padilla, N, Palanque-Delabrouille, N, Palicio, PA, Pan, H-A, Pan, K, Parker, J, Paviot, R, Peirani, S, Ramrez, KP, Penny, S, Percival, WJ, Perez-Fournon, I, Perez-Rafols, I, Petitjean, P, Pieri, MM, Pinsonneault, M, Poovelil, VJ, Povick, JT, Prakash, A, Price-Whelan, AM, Raddick, MJ, Raichoor, A, Ray, A, Rembold, SB, Rezaie, M, Riffel, RA, Riffel, R, Rix, H-W, Robin, AC, Roman-Lopes, A, Roman-Zuniga, C, Rose, B, Ross, AJ, Rossi, G, Rowlands, K, Rubin, KHR, Salvato, M, Sanchez, AG, Sanchez-Menguiano, L, Sanchez-Gallego, JR, Sayres, C, Schaefer, A, Schiavon, RP, Schimoia, JS, Schlafly, E, Schlegel, D, Schneider, DP, Schultheis, M, Schwope, A, Seo, H-J, Serenelli, A, Shafieloo, A, Shamsi, SJ, Shao, Z, Shen, S, Shetrone, M, Shirley, R, Aguirre, VS, Simon, JD, Skrutskie, MF, Slosar, A, Smethurst, R, Sobeck, J, Sodi, BC, Souto, D, Stark, DV, Stassun, KG, Steinmetz, M, Stello, D, Stermer, J, Storchi-Bergmann, T, Streblyanska, A, Stringfellow, GS, Stutz, A, Suarez, G, Sun, J, Taghizadeh-Popp, M, Talbot, MS, Tayar, J, Thakar, AR, Theriault, R, Thomas, D, Thomas, ZC, Tinker, J, Tojeiro, R, Toledo, HH, Tremonti, CA, Troup, NW, Tuttle, S, Unda-Sanzana, E, Valentini, M, Vargas-Gonzalez, J, Vargas-Magana, M, Vazquez-Mata, JA, Vivek, M, Wake, D, Wang, Y, Weaver, BA, Weijmans, A-M, Wild, V, Wilson, JC, Wilson, RF, Wolthuis, N, Wood-Vasey, WM, Yan, R, Yang, M, Yeche, C, Zamora, O, Zarrouk, P, Zasowski, G, Zhang, K, Zhao, C, Zhao, G, Zheng, Z, Zheng, Z, Zhu, G & Zou, H 2020, 'The 16th Data Release of the Sloan Digital Sky Surveys: first release from the APOGEE-2 Southern Survey and full release of eBOSS spectra', *Astrophysical Journal. Supplement Series*, vol. 249, no. 1, 3. https://doi.org/10.3847/1538-4365/ab929e

The Astrophysical Journal Supplement Series, 249:3 (21pp), 2020 July https://doi.org/10.3847/1538-4365/ab929e

The 16th Data Release of the Sloan Digital Sky Surveys: First Release from the APOGEE-2 Southern Survey and Full Release of eBOSS Spectra

Romina Ahumada[1], Carlos Allende Prieto[2,3], Andrés Almeida[4], Friedrich Anders[5,6], Scott F. Anderson[7], Brett H. Andrews[8], Borja Anguiano[9], Riccardo Arcodia[10], Eric Armengaud[11], Marie Aubert[12], Santiago Avila[13,14], Vladimir Avila-Reese[15], Carles Badenes[8], Christophe Balland[16], Kat Barger[17], Jorge K. Barrera-Ballesteros[15], Sarbani Basu[18], Julian Bautista[19], Rachael L. Beaton[20], Timothy C. Beers[21], B. Izamar T. Benavides[22], Chad F. Bender[23], Mariangela Bernardi[24], Matthew Bershady[25,26], Florian Beutler[19], Christian Moni Bidin[1], Jonathan Bird[27], Dmitry Bizyaev[28,29], Guillermo A. Blanc[20], Michael R. Blanton[30], Médéric Boquien[31], Jura Borissova[32,33], Jo Bovy[34,35], W. N. Brandt[36,37,38], Jonathan Brinkmann[28], Joel R. Brownstein[39], Kevin Bundy[40], Martin Bureau[41], Adam Burgasser[42], Etienne Burtin[11], Mariana Cano-Díaz[15], Raffaella Capasso[43,44,45], Michele Cappellari[41], Ricardo Carrera[46], Solène Chabanier[11], William Chaplin[47], Michael Chapman[48], Brian Cherinka[49], Cristina Chiappini[5], Peter Doohyun Choi[50], S. Drew Chojnowski[51], Haeun Chung[52], Nicolas Clerc[53], Damien Coffey[10], Julia M. Comerford[54], Johan Comparat[10], Luiz da Costa[55,56], Marie-Claude Cousinou[12], Kevin Covey[57], Jeffrey D. Crane[20], Katia Cunha[23,56], Gabriele da Silva Ilha[55,58], Yu Sophia Dai (戴昱)[59], Sanna B. Damsted[60], Jeremy Darling[54], James W. Davidson, Jr.[9], Roger Davies[41], Kyle Dawson[39], Nikhil De[17,61], Axel de la Macorra[22], Nathan De Lee[27,62], Anna Bárbara de Andrade Queiroz[5], Alice Deconto Machado[55,58], Sylvain de la Torre[63], Flavia Dell'Agli[2,3], Hélion du Mas des Bourboux[39], Aleksandar M. Diamond-Stanic[64], Sean Dillon[65,66], John Donor[17], Niv Drory[67], Chris Duckworth[68], Tom Dwelly[10], Garrett Ebelke[9], Sarah Eftekharzadeh[39], Arthur Davis Eigenbrot[25], Yvonne P. Elsworth[47], Mike Eracleous[36,37], Ghazaleh Erfanianfar[10], Stephanie Escoffier[12], Xiaohui Fan[23], Emily Farr[7], José G. Fernández-Trincado[69,70], Diane Feuillet[71,72], Alexis Finoguenov[60], Patricia Fofie[65,73], Amelia Fraser-McKelvie[74], Peter M. Frinchaboy[17], Sebastien Fromenteau[75], Hai Fu[76], Lluís Galbany[8], Rafael A. Garcia[11,77], D. A. García-Hernández[2,3], Luis Alberto Garma Oehmichen[15], Junqiang Ge[59], Marcio Antonio Geimba Maia[55,56], Doug Geisler[4,78,79], Joseph Gelfand[80], Julian Goddy[65], Violeta Gonzalez-Perez[19,81], Kathleen Grabowski[28], Paul Green[82], Catherine J. Grier[23,36,37], Hong Guo[83], Julien Guy[84], Paul Harding[85], Sten Hasselquist[39,136], Adam James Hawken[12], Christian R. Hayes[9], Fred Hearty[36], S. Hekker[86,87], David W. Hogg[30], Jon A. Holtzman[51], Danny Horta[81], Jiamin Hou[10], Bau-Ching Hsieh[88], Daniel Huber[89], Jason A. S. Hunt[35], J. Ider Chitham[10], Julie Imig[51], Mariana Jaber[22], Camilo Eduardo Jimenez Angel[2,3], Jennifer A. Johnson[90], Amy M. Jones[91], Henrik Jönsson[92,72], Eric Jullo[63], Yerim Kim[50], Karen Kinemuchi[28], Charles C. Kirkpatrick IV[60], George W. Kite[19], Mark Klaene[28], Jean-Paul Kneib[63,93], Juna A. Kollmeier[20], Hui Kong[90], Marina Kounkel[57], Dhanesh Krishnarao[25], Ivan Lacerna[69,94], Ting-Wen Lan[95], Richard R. Lane[69,96], David R. Law[49], Jean-Marc Le Goff[11], Henry W. Leung[34], Hannah Lewis[9], Cheng Li[97], Jianhui Lian[19], Lihwai Lin (林俐暉)[88], Dan Long[28], Penélope Longa-Peña[31], Britt Lundgren[98], Brad W. Lyke[99], J. Ted Mackereth[47], Chelsea L. MacLeod[82], Steven R. Majewski[9], Arturo Manchado[2,3,100], Claudia Maraston[19], Paul Martini[90,101], Thomas Masseron[2,3], Karen L. Masters (何凱論)[65,137], Savita Mathur[2,3], Richard M. McDermid[102], Andrea Merloni[10], Michael Merrifield[74], Szabolcs Mészáros[103,104,138], Andrea Miglio[47], Dante Minniti[33,105,106], Rebecca Minsley[64], Takamitsu Miyaji[107], Faizan Gohar Mohammad[48], Benoit Mosser[108], Eva-Maria Mueller[19,41], Demitri Muna[90], Andrea Muñoz-Gutiérrez[22], Adam D. Myers[99], Seshadri Nadathur[19], Preethi Nair[91], Kirpal Nandra[10], Janaina Correa do Nascimento[55,109], Rebecca Jean Nevin[54], Jeffrey A. Newman[8], David L. Nidever[110,111], Christian Nitschelm[31], Pasquier Noterdaeme[112], Julia E. O'Connell[17,78], Matthew D. Olmstead[113], Daniel Oravetz[28], Audrey Oravetz[28], Yeisson Osorio[2,3], Zachary J. Pace[25], Nelson Padilla[96], Nathalie Palanque-Delabrouille[11], Pedro A. Palicio[2,3], Hsi-An Pan[71,88], Kaike Pan[28], James Parker[28], Romain Paviot[12,63], Sebastien Peirani[112], Karla Peña Ramírez[31], Samantha Penny[19], Will J. Percival[48,114,115], Ismael Perez-Fournon[2,3], Ignasi Pérez-Ràfols[63], Patrick Petitjean[112], Matthew M. Pieri[63], Marc Pinsonneault[101], Vijith Jacob Poovelil[39], Joshua Tyler Povick[110], Abhishek Prakash[116], Adrian M. Price-Whelan[117,118], M. Jordan Raddick[119], Anand Raichoor[93], Amy Ray[17], Sandro Barboza Rembold[55,58], Mehdi Rezaie[120], Rogemar A. Riffel[55,58], Rogério Riffel[55,109], Hans-Walter Rix[71], Annie C. Robin[70], A. Roman-Lopes[79], Carlos Román-Zúñiga[107], Benjamin Rose[49], Ashley J. Ross[90], Graziano Rossi[50], Kate Rowlands[49,119], Kate H. R. Rubin[121], Mara Salvato[10], Ariel G. Sánchez[10], Laura Sánchez-Menguiano[2,3], José R. Sánchez-Gallego[7], Conor Sayres[7], Adam Schaefer[25], Ricardo P. Schiavon[81], Jaderson S. Schimoia[109], Edward Schlafly[84], David Schlegel[84], Donald P. Schneider[36,37], Mathias Schultheis[122], Axel Schwope[5], Hee-Jong Seo[120], Aldo Serenelli[123,124], Arman Shafieloo[125,126], Shoaib Jamal Shamsi[65], Zhengyi Shao[83], Shiyin Shen[83], Matthew Shetrone[127], Raphael Shirley[2,3], Víctor Silva Aguirre[87], Joshua D. Simon[20], M. F. Skrutskie[9], Anže Slosar[128], Rebecca Smethurst[41], Jennifer Sobeck[7], Bernardo Cervantes Sodi[129], Diogo Souto[56,130], David V. Stark[65,95], Keivan G. Stassun[27], Matthias Steinmetz[5], Dennis Stello[131], Julianna Stermer[16], Thaisa Storchi-Bergmann[55,109], Alina Streblyanska[2], Guy S. Stringfellow[54], Amelia Stutz[78], Genaro Suárez[107], Jing Sun[17], Manuchehr Taghizadeh-Popp[119], Michael S. Talbot[39], Jamie Tayar[89], Aniruddha R. Thakar[119], Riley Theriault[64], Daniel Thomas[19], Zak C. Thomas[19],

Jeremy Tinker[30], Rita Tojeiro[68], Hector Hernandez Toledo[15], Christy A. Tremonti[25], Nicholas W. Troup[9], Sarah Tuttle[7], Eduardo Unda-Sanzana[31], Marica Valentini[5], Jaime Vargas-González[132], Mariana Vargas-Magaña[22], Jose Antonio Vázquez-Mata[15], M. Vivek[36], David Wake[98], Yuting Wang[59], Benjamin Alan Weaver[111], Anne-Marie Weijmans[68], Vivienne Wild[68], John C. Wilson[9], Robert F. Wilson[9], Nathan Wolthuis[65], W. M. Wood-Vasey[8], Renbin Yan[133], Meng Yang[68], Christophe Yèche[11], Olga Zamora[2,3], Pauline Zarrouk[134], Gail Zasowski[39], Kai Zhang[84], Cheng Zhao[93], Gongbo Zhao[19,59,135], Zheng Zheng[39], Zheng Zheng[59], Guangtun Zhu[119], and Hu Zou[59]

[1] Instituto de Astronomía, Universidad Católica del Norte, Av. Angamos 0610, Antofagasta, Chile; spokesperson@sdss.org
[2] Instituto de Astrofísica de Canarias (IAC), C/ Via Láctea s/n, E-38205 La Laguna, Tenerife, Spain
[3] Universidad de La Laguna (ULL), Departamento de Astrofísica, E-38206 La Laguna, Tenerife Spain
[4] Instituto de Investigación Multidisciplinario en Ciencia y Tecnología, Universidad de La Serena. Avenida Raúl Bitrán S/N, La Serena, Chile
[5] Leibniz-Institut für Astrophysik Potsdam (AIP), An der Sternwarte 16, D-14482 Potsdam, Germany
[6] Institut de Ciències del Cosmos, Universitat de Barcelona (IEEC-UB), Carrer Martí i Franquès 1, E-08028 Barcelona, Spain
[7] Department of Astronomy, University of Washington, Box 351580, Seattle, WA 98195, USA
[8] PITT PACC, Department of Physics and Astronomy, University of Pittsburgh, Pittsburgh, PA 15260, USA
[9] Department of Astronomy, University of Virginia, Charlottesville, VA 22904-4325, USA
[10] Max-Planck-Institut für extraterrestrische Physik, Gießenbachstraße 1, D-85748 Garching, Germany
[11] IRFU, CEA, Université Paris-Saclay, F-91191 Gif-sur-Yvette, France
[12] Aix Marseille Université, CNRS/IN2P3, CPPM, Marseille, France
[13] Departamento de Física Teórica, Facultad de Ciencias, Universidad Autónoma de Madrid, E-28049 Cantoblanco, Madrid, Spain
[14] Instituto de Física Teórica, UAM-CSIC, Universidad Autonoma de Madrid, E-28049 Cantoblanco, Madrid, Spain
[15] Instituto de Astronomía, Universidad Nacional Autónoma de México, A.P. 70-264, 04510, Mexico, D.F., México
[16] Sorbonne Université, CNRS/IN2P3, Laboratoire de Physique Nucléaire et de Hautes Energies (LPNHE), 4 Place Jussieu, F-75252 Paris, France
[17] Department of Physics & Astronomy, Texas Christian University, Fort Worth, TX 76129, USA
[18] Yale Center for Astronomy and Astrophysics, Yale University, New Haven, CT, 06520, USA
[19] Institute of Cosmology & Gravitation, University of Portsmouth, Dennis Sciama Building, Portsmouth, PO1 3FX, UK
[20] The Observatories of the Carnegie Institution for Science, 813 Santa Barbara Street, Pasadena, CA 91101, USA
[21] Department of Physics and JINA Center for the Evolution of the Elements, University of Notre Dame, Notre Dame, IN 46556, USA
[22] Instituto de Física Universidad Nacional Autónoma de México, Apdo. Postal 20-364, México
[23] Steward Observatory, University of Arizona, 933 North Cherry Avenue, Tucson, AZ 85721-0065, USA
[24] Department of Physics and Astronomy, University of Pennsylvania, Philadelphia, PA 19104, USA
[25] Department of Astronomy, University of Wisconsin-Madison, 475N. Charter Street, Madison WI 53703, USA
[26] South African Astronomical Observatory, P.O. Box 9, Observatory 7935, Cape Town, South Africa
[27] Department of Physics and Astronomy, Vanderbilt University, VU Station 1807, Nashville, TN 37235, USA
[28] Apache Point Observatory and New Mexico State University, P.O. Box 59, Sunspot, NM 88349, USA
[29] Sternberg Astronomical Institute, Moscow State University, 119992, Moscow, Russia
[30] Center for Cosmology and Particle Physics, Department of Physics, 726 Broadway, Room 1005, New York University, New York, NY 10003, USA
[31] Centro de Astronomía (CITEVA), Universidad de Antofagasta, Avenida Angamos 601, Antofagasta 1270300, Chile
[32] Instituto de Física y Astronomía, Universidad de Valparaíso, Av. Gran Bretaña 1111, Playa Ancha, Casilla 5030, Chile
[33] Millennium Institute of Astrophysics (MAS), Santiago, Chile
[34] Department of Astronomy and Astrophysics, University of Toronto, 50 St. George Street, Toronto, ON, M5S 3H4, Canada
[35] Dunlap Institute for Astronomy and Astrophysics, University of Toronto, 50 St. George Street, Toronto, Ontario M5S 3H4, Canada
[36] Department of Astronomy and Astrophysics, Eberly College of Science, The Pennsylvania State University, 525 Davey Laboratory, University Park, PA 16802, USA
[37] Institute for Gravitation and the Cosmos, Pennsylvania State University, University Park, PA 16802, USA
[38] Department of Physics, The Pennsylvania State University, University Park, PA 16802, USA
[39] Department of Physics and Astronomy, University of Utah, 115 S. 1400 E., Salt Lake City, UT 84112, USA
[40] UCO/Lick Observatory, University of California, Santa Cruz, 1156 High Street Santa Cruz, CA 95064, USA
[41] Sub-department of Astrophysics, Department of Physics, University of Oxford, Denys Wilkinson Building, Keble Road, Oxford OX1 3RH, UK
[42] Center for Astrophysics and Space Science, University of California San Diego, La Jolla, CA 92093, USA
[43] Faculty of Physics, Ludwig-Maximilians-Universität, Scheinerstr. 1, D-81679 Munich, Germany
[44] Excellence Cluster Universe, Boltzmannstr. 2, D-85748 Garching, Germany
[45] INAF-Osservatorio Astronomico di Trieste, via G. B. Tiepolo 11, I-34143 Trieste, Italy
[46] Astronomical Observatory of Padova, National Institute of Astrophysics, Vicolo Osservatorio I-5-35122—Padova, Italy
[47] School of Physics and Astronomy, University of Birmingham, Edgbaston, Birmingham B15 2TT, UK
[48] Waterloo Centre for Astrophysics, Department of Physics and Astronomy, University of Waterloo, Waterloo, ON N2L 3G1, Canada
[49] Space Telescope Science Institute, 3700 San Martin Drive, Baltimore, MD 21218, USA
[50] Department of Physics and Astronomy, Sejong University, 209, Neungdong-ro, Gwangjin-gu, Seoul, Republic of Korea
[51] Department of Astronomy, New Mexico State University, Las Cruces, NM 88003, USA
[52] Korean Institute for Advanced Study, 85 Hoegiro, Dongdaemun-gu, Seoul 130-722, Republic of Korea
[53] IRAP Institut de Recherche en Astrophysique et Planétologie, Université de Toulouse, CNRS, UPS, CNES, Toulouse, France
[54] Center for Astrophysics and Space Astronomy, Department of Astrophysical and Planetary Sciences, University of Colorado, 389 UCB, Boulder, CO 80309-0389, USA
[55] Laboratório Interinstitucional de e-Astronomia, 77 Rua General José Cristino, Rio de Janeiro, 20921-400, Brazil
[56] Observatório Nacional, Rio de Janeiro, Brazil
[57] Department of Physics and Astronomy, Western Washington University, 516 High Street, Bellingham, WA 98225, USA
[58] Departamento de Física, CCNE, Universidade Federal de Santa Maria, 97105-900, Santa Maria, RS, Brazil
[59] National Astronomical Observatories of China, Chinese Academy of Sciences, 20A Datun Road, Chaoyang District, Beijing 100012, People's Republic of China
[60] Department of Physics, University of Helsinki, Gustaf Hällströmin katu 2a, FI-00014 Helsinki, Finland
[61] Fort Worth Country Day, Fort Worth, TX 76109, USA
[62] Department of Physics, Geology, and Engineering Tech, Northern Kentucky University, Highland Heights, KY 41099, USA
[63] Aix Marseille Université, CNRS, LAM, Laboratoire d'Astrophysique de Marseille, Marseille, France
[64] Department of Physics and Astronomy, Bates College, 44 Campus Avenue, Lewiston ME 04240, USA

[65] Department of Physics and Astronomy, Haverford College, 370 Lancaster Ave, Haverford, PA 19041, USA
[66] Department of Physics, Chico State University, 400 W 1st St, Chico, CA 95929, USA
[67] McDonald Observatory, The University of Texas at Austin, 1 University Station, Austin, TX 78712, USA
[68] School of Physics and Astronomy, University of St Andrews, North Haugh, St. Andrews KY16 9SS, UK
[69] Instituto de Astronomía y Ciencias Planetarias, Universidad de Atacama, Copayapu 485, Copiapó, Chile
[70] The Observatoire des sciences de l'Universit/'e de Besançon, 41 Avenue de l'Observatoire, F-25000 Besançon, France
[71] Max-Planck-Institut für Astronomie, Königstuhl 17, D-69117 Heidelberg, Germany
[72] Lund Observatory, Department of Astronomy and Theoretical Physics, Lund University, Box 43, SE-22100 Lund, Sweden
[73] Astronomy Department, Williams College, Williamstown, MA 01267, USA
[74] School of Physics and Astronomy, University of Nottingham, University Park, Nottingham NG7 2RD, UK
[75] Instituto de Ciencias Fśicas (ICF), Universidad Nacional Autónoma de México, Av. Universidad s/n, Col. Chamilpa, Cuernavaca, Morelos, 62210, México
[76] Department of Physics & Astronomy, University of Iowa, Iowa City, IA 52245, USA
[77] AIM, CEA, CNRS, Université Paris-Saclay, Université Paris Diderot, Sorbonne Paris Cité, 91191 Gif-sur-Yvette, France
[78] Departmento de Astronomía, Universidad de Concepción, Casilla 160-C, Concepción, Chile
[79] Departamento de Astronomía, Facultad de Ciencias, Universidad de La Serena. Av. Juan Cisternas 1200, La Serena, Chile
[80] NYU Abu Dhabi, P.O. Box 129188, Abu Dhabi, UAE
[81] Astrophysics Research Institute, Liverpool John Moores University, IC2, Liverpool Science Park, 146 Brownlow Hill, Liverpool L3 5RF, UK
[82] Harvard-Smithsonian Center for Astrophysics, 60 Garden Street, MS 20, Cambridge, MA 02138, USA
[83] Shanghai Astronomical Observatory, Chinese Academy of Sciences, 80 Nandan Road, Shanghai 200030, People's Republic of China
[84] Lawrence Berkeley National Laboratory, 1 Cyclotron Road, Berkeley, CA 94720, USA
[85] Department of Astronomy, Case Western Reserve University, Cleveland, OH 44106, USA
[86] Max Planck Institute for Solar System Research, SAGE research group, Justus-von-Liebig-Weg 3, D-37077 Göttingen, Germany
[87] Stellar Astrophysics Centre, Department of Physics and Astronomy, Aarhus University, Ny Munkegade 120, DK-8000 Aarhus C, Denmark
[88] Academia Sinica Institute of Astronomy and Astrophysics, P.O. Box 23-141, Taipei 10617, Taiwan
[89] Institute for Astronomy, University of Hawai'i, 2680 Woodlawn Drive, Honolulu, HI 96822, USA
[90] Department of Physics and Center for Cosmology and AstroParticle Physics, The Ohio State University, Columbus, OH 43210, USA
[91] Department of Physics and Astronomy, University of Alabama, Tuscaloosa, AL 35487, USA
[92] Materials Science and Applied Mathematics, Malmö University, SE-205 06 Malmö, Sweden
[93] Institute of Physics, Laboratory of Astrophysics, Ecole Polytechnique Fédérale de Lausanne (EPFL), Observatoire de Sauverny, 1290 Versoix, Switzerland
[94] Instituto Milenio de Astrofísica, Av. Vicuña Mackenna 4860, Macul, Santiago, Chile
[95] Kavli Institute for the Physics and Mathematics of the Universe (WPI), University of Tokyo, Kashiwa 277-8583, Japan
[96] Instituto de Astrofísica, Pontificia Universidad Católica de Chile, Av. Vicuna Mackenna 4860, 782-0436 Macul, Santiago, Chile
[97] Tsinghua Center of Astrophysics & Department of Physics, Tsinghua University, Beijing 100084, People's Republic of China
[98] Department of Physics and Astronomy, University of North Carolina Asheville, One University Heights, Asheville, NC 28804, USA
[99] Department of Physics and Astronomy, University of Wyoming, Laramie, WY 82071, USA
[100] CSIC, Spain
[101] Department of Astronomy, The Ohio State University, 140 W. 18th Avenue, Columbus, OH 43210, USA
[102] Department of Physics and Astronomy, Macquarie University, Sydney NSW 2109, Australia
[103] ELTE Gothard Astrophysical Observatory, H-9704 Szombathely, Szent Imre herceg st. 112, Hungary
[104] MTA-ELTE Exoplanet Research Group, 9700 Szombathely, Szent Imre h. st. 112, Hungary
[105] Departamento de Ciencias Fisicas, Facultad de Ciencias Exactas, Universidad Andres Bello, Av. Fernandez Concha 700, Las Condes, Santiago, Chile
[106] Vatican Observatory, V00120 Vatican City State, Italy
[107] Instituto de Astronomía en Ensenada, Universidad Nacional Autónoma de México, Km. 107 Carr. Tijuana-Ensenada, BC 22760, México
[108] LESIA, Observatoire de Paris, Université PSL, CNRS, Sorbonne Université, Université de Paris, 5 place Jules Janssen, F-92195 Meudon, France
[109] Departamento de Astronomia, Instituto de Física, Universidade Federal do Rio Grande do Sul. Av. Bento Goncalves 9500, 91501-970, Porto Alegre, RS, Brasil
[110] Department of Physics, Montana State University, P.O. Box 173840, Bozeman, MT 59717-3840, USA
[111] NSF's National Optical-Infrared Astronomy Research Laboratory, 950 North Cherry Avenue, Tucson, AZ 85719, USA
[112] Institut d'Astrophysique de Paris, UMR 7095, SU-CNRS, 98bis bd Arago, F-75014 Paris, France
[113] King's College, 133 North River St, Wilkes Barre, PA 18711, USA
[114] Perimeter Institute for Theoretical Physics, Waterloo, ON N2L 2Y5, Canada
[115] Department of Physics and Astronomy, University of Waterloo, 200 University Ave W, Waterloo, ON N2L 3G1, Canada
[116] California Institute of Technology, MC 100-22, 1200 E California Boulevard, Pasadena, CA 91125, USA
[117] Department of Astrophysical Sciences, Princeton University, Princeton, NJ 08544, USA
[118] Center for Computational Astrophysics, Flatiron Institute, 162 Fifth Avenue, New York, NY, 10010, USA
[119] Center for Astrophysical Sciences, Department of Physics and Astronomy, Johns Hopkins University, 3400 North Charles Street, Baltimore, MD 21218, USA
[120] Department of Physics and Astronomy, Ohio University, Clippinger Labs, Athens, OH 45701, USA
[121] Department of Astronomy, San Diego State University, San Diego, CA 92182, USA
[122] Observatoire de la Côte d'Azur, Laboratoire Lagrange, F-06304 Nice Cedex 4, France
[123] Institute of Space Sciences (ICE, CSIC), Carrer de Can Magrans S/N, Campus UAB, Barcelona, E-08193, Spain
[124] Institut d'Estudis Espacials de Catalunya, C/Gran Capita, 2-4, E-08034, Barcelona, Spain
[125] Korea Astronomy and Space Science Institute, 776 Daedeokdae-ro, Yuseong-gu, Daejeon 305-348, Republic of Korea
[126] University of Science and Technology, 217 Gajeong-ro, Yuseong-gu, Daejeon 34-113, Republic of Korea
[127] UC Observatories, University of California Santa Cruz, 1156 High Street, Santa Cruz, CA 95064, USA
[128] Brookhaven National Laboratory, Upton, NY 11973, USA
[129] Instituto de Radioastronomía y Astrofísica, Universidad Nacional Autónoma de México, Campus Morelia, A.P. 3-72, C.P. 58089 Michoacán, México
[130] Departamento de Física, Universidade Federal de Sergipe, Av. Marechal Rondon, S/N, 49000-000 São Cristóvão, SE, Brazil
[131] School of Physics, UNSW Sydney, NSW 2052, Australia
[132] Centre for Astrophysics Research, School of Physics, Astronomy and Mathematics, University of Hertfordshire, College Lane, Hatfield AL10 9AB, UK

[133] Department of Physics and Astronomy, University of Kentucky, 505 Rose Street, Lexington, KY, 40506-0055, USA
[134] Institute for Computational Cosmology, Department of Physics, Durham University, South Road, Durham DH1 3LE, UK
[135] University of Chinese Academy of Sciences, Beijing, 100049, People's Republic of China
Received 2019 December 4; revised 2020 May 7; accepted 2020 May 11; published 2020 June 25

Abstract

This paper documents the 16th data release (DR16) from the Sloan Digital Sky Surveys (SDSS), the fourth and penultimate from the fourth phase (SDSS-IV). This is the first release of data from the Southern Hemisphere survey of the Apache Point Observatory Galactic Evolution Experiment 2 (APOGEE-2); new data from APOGEE-2 North are also included. DR16 is also notable as the final data release for the main cosmological program of the Extended Baryon Oscillation Spectroscopic Survey (eBOSS), and all raw and reduced spectra from that project are released here. DR16 also includes all the data from the Time Domain Spectroscopic Survey and new data from the SPectroscopic IDentification of ERosita Survey programs, both of which were co-observed on eBOSS plates. DR16 has no new data from the Mapping Nearby Galaxies at Apache Point Observatory (MaNGA) survey (or the MaNGA Stellar Library "MaStar"). We also preview future SDSS-V operations (due to start in 2020), and summarize plans for the final SDSS-IV data release (DR17).

Unified Astronomy Thesaurus concepts: Astronomy databases (83); Optical telescopes (1174); Infrared astronomy (786); Redshift surveys (1378); Galactic abundances (2002); Stellar spectral lines (1630); Stellar properties (1624)

1. Introduction

The Sloan Digital Sky Surveys (SDSS) have been observing the skies from Apache Point Observatory (APO) since 1998 (using the 2.5 m Sloan Foundation Telescope; Gunn et al. 2006) and from Las Campanas Observatory (LCO) since 2017 (using the du Pont 2.5 m Telescope).

Representing the fourth phase of the SDSS, SDSS-IV (Blanton et al. 2017) consists of three main surveys: the Extended Baryon Oscillation Spectroscopic Survey (eBOSS; Dawson et al. 2016), Mapping Nearby Galaxies at APO (MaNGA; Bundy et al. 2015), and the APO Galactic Evolution Experiment 2 (APOGEE-2; Majewski et al. 2017). Within eBOSS, SDSS-IV has also conducted two smaller programs: the SPectroscopic IDentification of ERosita Sources (SPIDERS; Clerc et al. 2016; Dwelly et al. 2017) and the Time Domain Spectroscopic Survey (TDSS; Morganson et al. 2015). These programs have investigated a broad range of cosmological scales, including cosmology with large-scale structure (LSS) in eBOSS, the population of variable quasars and stars with TDSS and X-ray detected active galactic nuclei (AGNs) and stars with SPIDERS, nearby galaxies in MaNGA, and the Milky Way and its stars in APOGEE-2.

This paper documents the 16th data release from the SDSS (DR16), the latest in a series that began in 2001 (Stoughton et al. 2002). It is the fourth data release from SDSS-IV (following DR13: Albareti et al. 2017; DR14: Abolfathi et al. 2018; DR15: Aguado et al. 2019). A complete overview of the scope of DR16 is provided in Section 2, and information on how to access the data can be found in Section 3. DR16 contains three important milestones.

1. The first data from APOGEE-2 South (APOGEE-2S), which is mapping the Milky Way in the Southern Hemisphere from the du Pont Telescope at LCO. With the SDSS now operating APOGEE instruments in two hemispheres, all major components of the Milky Way are accessible (see Section 4).
2. The first and final release of eBOSS spectra from the emission line galaxy (ELG) cosmology program. The entirety of this LSS survey was conducted in the interval between DR14 and DR16. Covering the redshift range $0.6 < z < 1.1$, the eBOSS ELG program represents the highest-redshift galaxy survey ever conducted within the SDSS.
3. The full and final release of spectra from the main observing program of eBOSS, completing that cosmological redshift survey. DR16 therefore marks the end of a 20 year stretch during which the SDSS performed a redshift survey of the LSS in the universe. Over this span, the SDSS produced a catalog of spectroscopic galaxy redshifts that is a factor of more than five larger than any other program. DR16 provides spectra along with usable redshifts for around 2.6 million unique galaxies. The catalogs that contain the information to accurately measure the clustering statistics of ELGs, luminous red galaxies (LRGs), quasars, and Lyα absorption will be released later (see Section 5).

DR16 also represents the full release of the TDSS subprogram, which in total releases spectra for 131,552 variable sources (see Section 5.4). The SPIDERS subprogram will have a small number of observations in the future to cover eROSITA targets, but DR16 releases a number of Value Added Catalogs (VACs) characterizing both X-ray cluster and X-ray point sources that have already been observed (as well as the optical spectra; see Section 5.3). There are no new data from MaNGA or MaStar (Yan et al. 2019) in DR16; however, a number of new or updated VACs based on DR15 MaNGA data are released (see Section 6).

2. Scope of DR16

Following the tradition of previous SDSS data releases, DR16 is a cumulative data release. This means that all previous data releases are included in DR16, and data products and catalogs of these previous releases will remain accessible on our data servers. Table 1 shows the number of spectra

[136] NSF Astronomy and Astrophysics Postdoctoral Fellow, USA.
[137] SDSS-IV Spokesperson.
[138] Premium Postdoctoral Fellow of the Hungarian Academy of Sciences.

Table 1
SDSS-IV Spectroscopic Data in DR13–DR16

Survey	Target Category	DR13	DR14	DR15	DR16
eBOSS					
	LRG samples	32,968	138,777	138,777	298,762
	ELG samples	14,459	35,094	35,094	269,889
	Main QSO sample	33,928	188,277	188,277	434,820
	Variability Selected QSOs	22,756	87,270	87,270	18,5816
	Other QSO samples	24,840	43,502	43,502	70,785
	TDSS targets	17,927	57,675	57,675	131,552
	SPIDERS targets	3133	16,394	16,394	36,300
	Reverberation mapping	849[a]	849[a]	849[a]	849[a]
	Standard stars/white dwarfs	53,584	63,880	63,880	84,605
APOGEE-2					
	Main red star sample	109,376	184,148	184,148	281,575
	AllStar entries	164,562	277,371	277,371	473,307[b]
	APOGEE-2S main red star sample	…	…	…	56,480
	APOGEE-2S AllStar entries	…	…	…	102,200
	APOGEE-2S contributed AllStar entries	…	…	…	37,409
	NMSU 1-meter AllStar entries	894	1018	1018	1071
	Telluric AllStar entries	17,293	27,127	27,127	34,016
	APOGEE-N commissioning stars	11,917	12,194	12,194	12,194
MaNGA					
	MaNGA Cubes	1390	2812	4824	4824
	MaNGA main galaxy sample:				
	`PRIMARY_v1_2`	600	1278	2126	2126
	`SECONDARY_v1_2`	473	947	1665	1665
	`COLOR-ENHANCED_v1_2`	216	447	710	710
	MaStar (MaNGA Stellar Library)	…	…	3326	3326
	Other MaNGA ancillary targets[c]	31	121	324	324

Notes.
[a] The number of reverberation mapping targets remains the same, but the number of visits increases.
[b] This number includes multiple entries for some stars; there are 437,485 unique stars.
[c] Many MaNGA ancillary targets were also observed as part of the main galaxy sample, and are counted twice in this table; some ancillary targets are not galaxies.

contained in DR16 along with those from previous releases and demonstrates the incremental gains with each release. We strongly advise to always use the most recent SDSS data release, as data will have been reprocessed using updated data reduction pipelines (DRPs), and catalogs may have been updated with new entries and/or improved analysis methods. These changes between DR16 and previous data releases are documented in this paper and on the DR16 website: https://www.sdss.org/dr16.

The content of DR16 is given by the following sets of data products.

1. eBOSS is releasing 860,935 new optical spectra of galaxies and quasars with respect to its previous SDSS data release. These targets were observed between MJD 57,520 (2016 May 11) and 58,543 (2019 March 1), and bring the total number of spectra observed by eBOSS to 1.4 million. This number includes spectra observed as part of the TDSS and SPIDERS sub-surveys, as well as the spectra taken as part of the eBOSS reverberation mapping (RM) ancillary program. All spectra, whether released previously or for the first time in this data release, have been processed using the latest version of the eBOSS DRP `v5_13_0`. In addition to the spectra, eBOSS is also releasing catalogs of redshifts, as well as various VACs (see Table 2). DR16 is the last SDSS data release that will contain new eBOSS spectra from the main program, as this survey has now finished. Additional observations of X-ray sources under the SPIDERS program and continued monitoring of quasars under the RM program are planned before the end of SDSS-IV, which will lead to another increment of single-fiber spectra from the Baryon Oscillation Spectroscopic Survey (BOSS) spectrograph in DR17.
2. APOGEE-2 is including 751,864 new infrared spectra;[139] The new spectra comprise both observations of 195,936 new stars and additional epochs on targets included in previous DRs. The majority of the stars are in the Milky Way (including Omega Centauri), but DR16 also contains stars from the Large and Small Magellanic Clouds and dwarf spheroidal satellites. A total of 262,997 spectra, for 102,200 unique stars, were obtained in the Southern Hemisphere from the APOGEE-S spectrograph at LCO. These new spectra were obtained from MJD 57,643 to MJD 58,301 (2016 September 12 to 2018 July 2) for APOGEE-2N from APO and from MJD 57,829 to MJD 58,358 (2017 March 17 to 2018 August 28) for APOGEE-2S from LCO. DR16 also includes all previously released APOGEE and APOGEE-2 spectra, which have been re-reduced with the latest version of the APOGEE data reduction and analysis pipeline. In addition to the reduced

[139] The number of entries in the All Visit file, which is larger than the number of combined spectra having entries in the AllStar file as listed in Table 1.

Table 2
New or Updated VACs

Description	Section	Reference(s)
APOGEE-2 red clumps	Section 4.5.1	Bovy et al. (2014)
APOGEE-2 `astroNN`	Section 4.5.2	Leung & Bovy (2019a)
APOGEE-2 *Joker*	Section 4.5.3	Price-Whelan et al. (2017, 2018, 2020)
APOGEE-2 OCCAM	Section 4.5.4	Donor et al. (2018, 2020)
APOGEE-2 StarHorse	Section 4.5.5	Queiroz et al. (2018); Anders et al. (2019); Queiroz et al. (2020)
eBOSS ELG classification	Section 5.1.3	Zhang et al. (2019)
SDSS galaxy single fiber FIREFLY	Section 5.1.3	Comparat et al. (2017)
SPIDERS X-ray clusters	Section 5.3.4	Clerc et al. (2016); C. Kirkpatrick et al. (2020, in preparation)
SPIDERS Rosat and XMM[a]-slew sources	Section 5.3.5	Comparat et al. (2020)
SPIDERS multiwavelength properties of RASS and XMMSL AGNs	Section 5.3.6	Comparat et al. (2020)
SPIDERS black hole masses	Section 5.3.7	Coffey et al. (2019)
MaNGA stellar masses from principal component analysis	Section 6.1	Pace et al. (2019a, 2019b)
MaNGA `PawlikMorph`	Section 6.2	Pawlik et al. (2016)

Note.
[a] X-ray Multi-Mirror Mission

spectra, element abundances and stellar parameters are included in this data release. APOGEE-2 is also releasing a number of VACs (Table 2)

3. MaNGA and MaStar are not releasing any new spectra in this data release; the spectra and data products included in DR16 are therefore identical to those that were released in DR15. However, MaNGA is contributing a number of of new or updated VACs in DR16, which are based on the DR15 sample and data products (see Table 2).
4. Since SDSS data releases are cumulative, DR16 also includes data from all previous SDSS data releases. All BOSS and eBOSS, APOGEE, and APOGEE-2 spectra that were previously released have all been reprocessed with the latest reduction and analysis pipelines. The MaNGA and MaStar data in DR16 are identical to those in DR15 (Aguado et al. 2019); SDSS-III MARVELS spectra have not changed since DR12 (Alam et al. 2015). SDSS Legacy Spectra in DR16 are the same as those released in their final form in DR8 (Aihara et al. 2011), and the SEGUE-1 and SEGUE-2 survey data in DR16 are identical to the final reductions released with DR9 (Ahn et al. 2012). The SDSS imaging had its most recent change in DR13 (Albareti et al. 2017), when it was recalibrated for eBOSS imaging purposes and DR16 contains this version of the imaging.

An overview of the total spectroscopic content of DR16, with number of spectra included, is given in Table 1. An overview of the VACs that are new or updated in DR16 can be found in Table 2; adding these to the VACs previously released in the SDSS gives a total of 46 VACs in DR16.[140]

3. Data Access

The SDSS data products included in DR16 are publicly available through several different channels. The best way to access the data products depends on the particular product, and the goal of the user. The different access options are described on the SDSS website: https://www.sdss.org/dr16/data_access/, and we also describe them below. We provide a variety of tutorials and examples for accessing data products online at https://www.sdss.org/dr16/tutorials/.

All software that was used by SDSS to reduce and process data, as well as to construct derived data products, is publicly available in either SVN or Github repositories; an overview of available software and where to retrieve it is given on https://www.sdss.org/dr16/software/.

3.1. Science Archive Server

The main path to access the raw and reduced imaging and spectroscopic data directly, as well as obtain intermediate data products and VACs, is through the SDSS Science Archive Server (SAS, https://data.sdss.org/sas/). Note that all previous data releases are also available on this server, but we recommend that users always adopt the latest data release, as these are reduced with the latest versions of the data reduction software. The SAS is a file-based system, which allows data downloads by browsing or through tools such as `rsync`, `wget` and Globus Online (see https://www.sdss.org/dr16/data_access/bulk for more details). The content of each data product on the SAS is outlined in its data model, which can be accessed through https://data.sdss.org/datamodel/.

3.2. Science Archive Webapp

Most of the reduced images and spectra on the SAS are also accessible through the Science Archive Webapp (SAW), which provides the user with options to display spectra and overlay model fits. The SAW includes search options to access specific subsamples of spectra, e.g., based on coordinates, redshift, and/or observing programs. Searches can also be saved as "permalinks" to allow sharing with collaborators and future use. Links are provided to download the spectra directly from the SAS, and to open SkyServer Explore pages for the objects displayed (see below for a description of the SkyServer). The SAW contains imaging, optical single-fiber spectra (SDSS-I/II, SEGUE, BOSS, eBOSS), infrared spectra (APOGEE-1/2), and stellar spectra of the MaStar stellar library. All of these webapps are linked from https://dr16.sdss.org/. Just like the SAS, the SAW provides access to previous data releases (back to DR8).

[140] That is 40 previous released VACs, seven of which are updated in DR16, and six VACs new to DR16.

3.3. Marvin for MaNGA

Integral-field spectroscopic data (MaNGA) are not available in the SAW because they follow a different data format from the single-object spectra. Instead, the MaNGA data can be accessed through Marvin (https://dr16.sdss.org/marvin/; Cherinka et al. 2019). Marvin can be used to both visualize and analyze MaNGA data products and perform queries on MaNGA metadata remotely. Marvin also contains a suite of Python tools, available through pip-install, that simplify interacting with the MaNGA data products and metadata. More information, including installation instructions for Marvin, can be found here: https://sdss-marvin.readthedocs.io/en/stable/. In DR16, although no new MaNGA data products are included, Marvin has been upgraded by providing access to a number of MaNGA VACs based on DR15 data.

3.4. Catalog Archive Server

The SDSS catalogs can be found and queried on the Catalog Archive Server (CAS; Thakar et al. 2008). These catalogs contain photometric and spectroscopic properties, as well as derived data products. Several value-added catalogs are also available on the CAS. For quick inspection of objects or small queries, the SkyServer webapp (https://skyserver.sdss.org) is the recommended route to access the catalogs: it contains among other facilities the Quick Look and Explore tools, as well as the option for SQL queries in synchronous mode directly in the browser. The SkyServer also contains tutorials and examples of SQL syntax (http://skyserver.sdss.org/public/en/help/docs/docshome.aspx). For larger queries, CASJobs (https://skyserver.sdss.org/casjobs) should be used, as it allows for asynchronous queries in batch mode. Users of CASJobs will need to create a (cost-free) personal account, which comes with storage space for query results (Li & Thakar 2008). A third way to access the SDSS catalogs is through the SciServer (https://www.sciserver.org), which is integrated with the CAS. SciServer allows users to run Jupyter notebooks in Docker containers, among other services.

3.5. Data Access for Education

We are providing access to a growing set of Jupyter notebooks that have been developed for introductory[141] and upper-level[142] university astronomy laboratory courses. These Python-based activities are designed to be run on the SciServer platform,[143] which enables the analysis and visualization of the vast SDSS data set from a web browser, without requiring any additional software or data downloads.

Additionally, Voyages (http://voyages.sdss.org/) provides activities and resources to help younger audiences explore the SDSS data. Voyages has been specifically developed to be used in secondary schools, and contains pointers to K-12 US science standards. A Spanish language version of these resources is now available at http://voyages.sdss.org/es.

4. APOGEE-2: First Release of Southern Hemisphere Data, and More from the North

APOGEE is performing a chemodynamical investigation across the entire Milky Way with two similarly designed near-infrared, high-resolution multiplexed spectrographs. DR16 constitutes the fifth release of data from APOGEE, which has run in two phases (APOGEE-1 and APOGEE-2) spanning both SDSS-III and SDSS-IV. For approximately three years (2011 August–2014 July), APOGEE-1 survey observations were conducted at the 2.5 m Sloan Foundation Telescope at APO as part of SDSS-III. In 2014 August, at the start of SDSS-IV, APOGEE-2 continued data acquisition at the APO Northern Hemisphere site (APOGEE-2N). With the construction of a second spectrograph (Wilson et al. 2019), APOGEE-2 commenced Southern Hemisphere operations at the 2.5 m Iréné du Pont Telescope at LCO (APOGEE-2S) in 2017 April. Majewski et al. (2017) provides an overview of the APOGEE-1 Survey (with a forthcoming planned overview of the APOGEE-2 Survey; S. Majewski et al. 2020, in preparation).

In detail, the APOGEE data in DR16 encompass all SDSS-III APOGEE-1 data and SDSS-IV APOGEE-2 data acquired with both instruments through 2018 August. The current release includes two additional years of APOGEE-2N data and almost doubles the number of stars with available spectra as compared to the previous public release (in DR14: Abolfathi et al. 2018). DR16 presents the first 16 months of data from APOGEE-2S. Thus, DR16 is the first release from APOGEE that includes data from across the entire night sky.

DR16 contains APOGEE data and information for 437,485 unique stars, including reduced and visit-combined spectra, radial velocity (RV) information, atmospheric parameters, and individual element abundances; nearly 1.8 million individual visit spectra are included. Figure 1 displays the APOGEE DR16 coverage in Galactic coordinates where each point represents a single "field" and is color-coded by the overall survey component (e.g., APOGEE, APOGEE-2N, and APOGEE-2S). Fields newly released in DR16 are encircled with black. As shown in this figure, the dual hemisphere view of APOGEE allows for targeting of all Milky Way components: the inner and outer halo, the four disk quadrants, and the full expanse of the bulge. The first APOGEE-2S observations of various Southern Hemisphere objects, such as Omega Centauri (l, $b = 309°$, $15°$) and our current targeting of the Large and Small Magellanic Clouds (l, $b = 280°$, $-33°$ and $303°$, $-44°$ respectively), are visible in Figure 1 as high-density areas of observation. Moreover, DR16 features substantially increased coverage at high Galactic latitudes as APOGEE continues to piggy-back on MaNGA-led observing during dark time. Figure 2 has the same projection, but uses color-coding to convey the number of unique targets for each of the APOGEE fields. Particularly dense regions include the Kepler field which serves multiple scientific programs, as well as APOGEE "deep" fields observed with multiple "cohorts" (see Zasowski et al. 2017). Detailed discussions of our targeting strategies for each Galactic component, as well as an evaluation of their efficacy, will be presented in forthcoming focused papers (R. Beaton et al. 2020, in preparation; F. Santana et al. 2020, in preparation).

4.1. APOGEE Southern Survey Overview

The APOGEE-2S Survey has been enabled by the construction of a second APOGEE spectrograph. The second instrument is a near duplicate of the first with comparable performance, simultaneously delivering 300 spectra in the H-band wavelength regime ($\lambda = 1.5$–$1.7\ \mu$m) at a resolution of $R \sim 22{,}500$. Slight differences occur between the two

[141] https://github.com/ritatojeiro/SDSSEPO
[142] https://github.com/brittlundgren/SDSS-EPO
[143] http://www.sciserver.org/

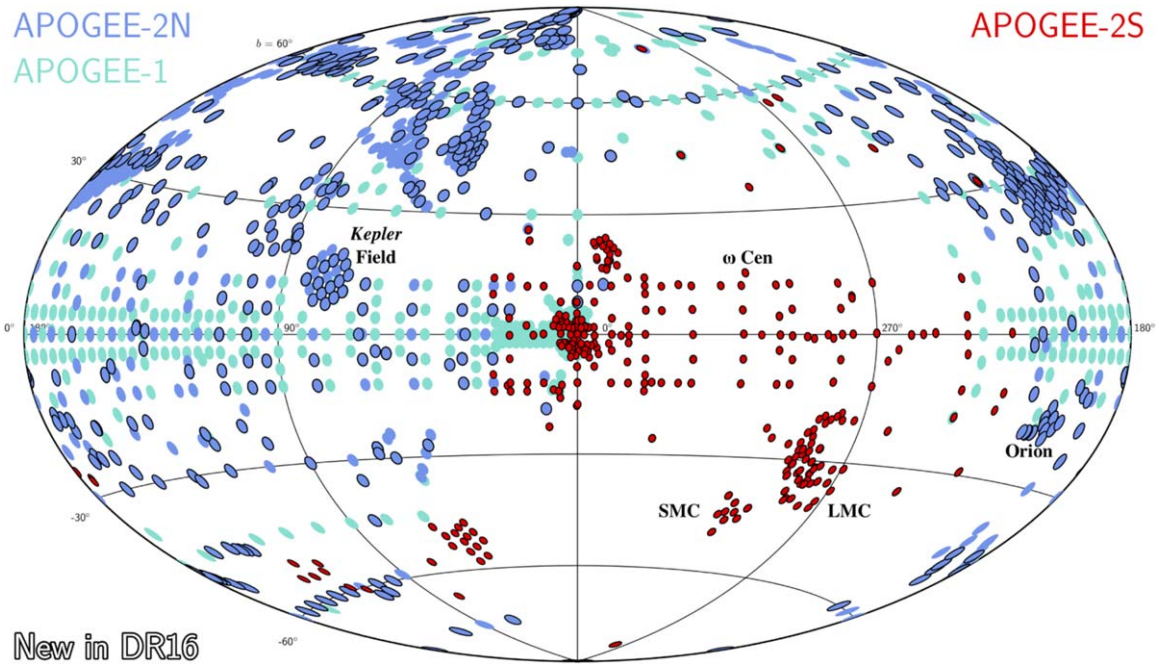

Figure 1. DR16 APOGEE sky coverage in Galactic coordinates. Each symbol represents a field, which is 7 square degrees for APOGEE-1 in cyan and APOGEE-2N in blue and 2.8 square degrees for APOGEE-2S in red (this difference is due to the different fields of view of the two telescopes; see Section 4.1). Fields that have new data presented in DR16 are highlighted with a black outline.

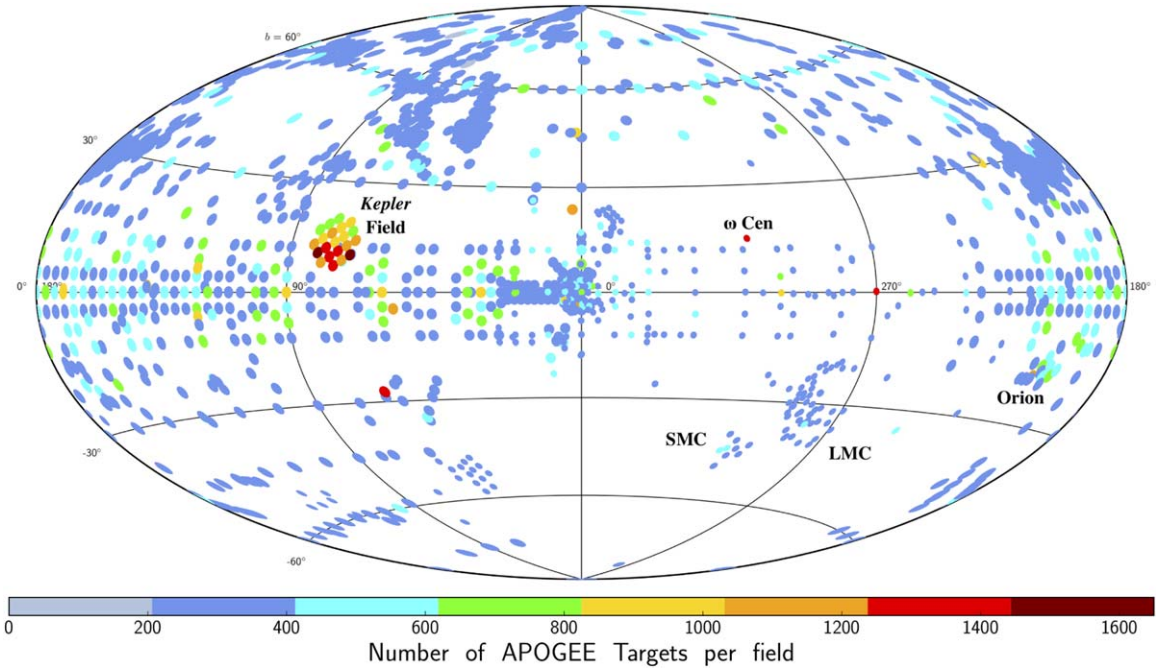

Figure 2. Sky map in Galactic coordinates showing the number of stars per APOGEE field (across APOGEE-1, 2N, and 2S). The disk is targeted with a symmetric dense grid within $|b| < 15°$. The dense coverage of the bulge and inner Galaxy is for $l < 30°$. Other special programs, like the Kepler-2 follow-up, have initial data in DR16. The circle sizes reflect the different fields of view of APOGEE-N and APOGEE-S; see Section 4.1.

instruments with respect to image quality and resolution across the detectors as described in detail in Wilson et al. (2019).

The telescopes of the Northern and Southern Hemisphere sites have the same apertures. However, because the du Pont telescope was designed with a slower focal ratio ($f/7.5$) than the Sloan Foundation telescope ($f/5$), the resulting field of view for APOGEE-2S is smaller than that for APOGEE-2N and the fibers subtend a smaller angular area. The difference in field of view is evident in Figure 1 by comparing the size of the red points (LCO fields) to those shown in blue or cyan (APO fields). However, the image quality (seeing) at LCO is generally better than that at APO, and this roughly compensates

for the smaller angular diameter fibers such that the typical throughput at LCO is similar to, or even better than, that obtained at APO.

4.2. General APOGEE Targeting

Extensive descriptions of the target selection and strategy are found in Zasowski et al. (2013) for APOGEE-1 and in Zasowski et al. (2017) for APOGEE-2. Details about the final selection method used for APOGEE-2N and APOGEE-2S will be presented in R. Beaton, et al. (2020, in preparation) and F. Santana et al. (2020, in preparation), respectively. These papers will provide descriptions for the ancillary and external programs, modifications to original targeting strategies required by evaluation of their effectiveness, and modifications of the field plan as required by weather gains or losses. We include all targeting information using flags and also provide input catalogs on the SAS.

APOGEE-2 scientific goals are implemented in a three-tier strategy, where individual programs aimed at specific science goals are classified as core, goal, or ancillary. The core programs produce a systematic exploration of the major components of the bulge, disk, and halo and are given the highest priority for implementation. The goal programs have more focused science goals, for example follow-up of Kepler Objects of Interest, and are implemented as a secondary priority. Ancillary programs are implemented at the lowest priority; such programs were selected from a competitive proposal process and have only been implemented for APOGEE-2N. Generally, the APOGEE-2N and APOGEE-2S survey science are implemented in the same manner.

In addition to a target selection analogous to that for the northern observations, APOGEE-2S includes external programs selected by the Chilean National Time Allocation Committee or the Observatories of the Carnegie Institution for Science and led by individual scientists (or teams) who can be external to the SDSS-IV collaboration. External programs can be "contributed," or proprietary; contributed data are processed through the normal APOGEE DRPs and are released along with other APOGEE data whereas proprietary programs are not necessarily processed through the standard pipelines or released with the public DRs.[144] The selection of external program targets does not follow the standard APOGEE survey criteria in terms of signal-to-noise ratio (S/N) or even source catalogs; the scientists involved were able to exercise great autonomy in target selection (e.g., no implementation of color cuts). External programs are implemented as classical observing programs with observations only occurring for a given program on nights assigned to it.

The APOGEE portion of DR16 includes 437,485 unique stars. Among these, 308,000 correspond to core science targets, 112,000 to goal science targets, 13,000 to ancillary APOGEE-2N program targets, and 37,000 to APOGEE-2S external program targets. These numbers add up to more than 437,485 due to some stars being in multiple categories.

4.3. APOGEE DR16 Data Products

The basic procedure for processing and analysis of APOGEE data is similar to that of DR14 data (Abolfathi et al. 2018; Holtzman et al. 2018), but a few notable differences are highlighted here. Full details, including verification analyses, are presented in Jönsson et al. (2020).

4.3.1. Spectral Reduction and RV Determinations

Nidever et al. (2015) describes the reduction procedure for APOGEE data. While the basic reduction steps for DR16 were the same as described there, improvements were implemented in the handling of bad pixels, flat-fielding, and wavelength calibration, all of which were largely motivated by small differences between the data produced by the APOGEE-S and APOGEE-N instruments. As an improvement over DR14, an attempt was made to provide rough relative flux calibration for the spectra. This was achieved by using observations of hot stars on the fiber plug plate for which the spectral energy distribution are known.

RVs were determined, as in DR14, using cross-correlation against a reference grid, but a new synthetic grid was calculated for the reference grid, using the same updated models that were used for the derivation of stellar parameters and abundances (see Section 4.3.2 for details). No constraint was placed on the effective temperature range of the synthetic grid based on the $J - K$ color; DR14 used such a constraint which led to a few issues with bad radial velocities. Therefore DR16 improves on this.

For the faintest stars in DR16, especially those in dwarf spheroidal galaxies, the individual visit spectra can have low S/N and, as a result, the RV determination fails. In many, but not all, cases, such objects are flagged as having bad or suspect RV combination. Users who are working with data for stars with $H > 14.5$ need to be very careful with these data, as incorrect RVs lead to incorrect spectral combination, which invalidates any subsequent analysis. We intend to remedy this problem in the next DR.

4.3.2. Atmospheric Parameter and Element Abundance Derivations

Stellar parameters and abundances are determined using the APOGEE Stellar Parameters and Chemical Abundance Pipeline (ASPCAP; García Pérez et al. 2016).[145] For DR16, entirely new synthetic grids were created for this analysis. These grids were based on a complete set of stellar atmospheres from the MARCS group (Gustafsson et al. 2008) that covers a wide range of $T_{\rm eff}$, $\log g$, [Fe/H], [α/M], and [C/M]. Spectral syntheses were performed using the Turbospectrum code (Plez 2012). The synthesis was done using a revised APOGEE line-list which was derived, as before, from matching very high-resolution spectra of the Sun and Arcturus. The revised line-list differs from that used previously by the inclusion of lines from FeH, Ce II, and Nd II, some revisions in the adopted Arcturus abundances, and a proper handling of the synthesis of a center-of-disk solar spectrum. Details on the line-list will be presented in V. Smith et al. (2020, in preparation). The synthetic grid for red giants was calculated with seven dimensions, including [N/M] and microturbulent velocity, as well as the atmospheric parameters previously listed; the range for [C/M] and [N/M] was expanded over that used for DR14. For the giants, the [C/Fe] grid was expanded to include -1.25 and -1.50 dex and the [N/Fe] dimension to cover from -0.50 to $+1.50$ dex. For dwarfs, an additional dimension was included to account for stellar rotation that included seven

[144] To date all external programs have been "contributed" so there are no proprietary external programs.

[145] https://github.com/sdss/apogee

steps (these being $v \sin i$ of 1.5, 3.0, 6.0, 12.0, 24.0, 48.0, and 96.0 km s^{-1}). During the stellar parameter and abundance fits, regions in the spectrum that were not well matched in the solar and Arcturus spectra were masked. The full details of the spectral grid derivations will be given in a dedicated paper on the APOGEE DR16 pipeline (Jönsson et al. 2020).

The DR16 analysis improves on the measurement of carbon and nitrogen abundances in dwarf stars over DR14, as DR16 includes separate [C/M] and [N/M] dimensions for dwarfs.

As for previous data releases, stellar parameters were determined by searching for the best fit in the synthetic grid. The method used to normalize the observed and model spectra was improved from previous releases, and a new minimization option was adopted in the FERRE code (Allende Prieto et al. 2006).[146] More details on these changes are given in Jönsson et al. (2020). As in previous releases, after the stellar parameters have been determined, these are held fixed while determining the elemental abundances; for these, only windows in the spectra that are sensitive to the element in question are fit, and only a single relevant abundance dimension of the grid is varied. The windows are chosen based on where our synthetic spectra are sensitive to a given element, and at the same time *not* sensitive to another element in the same abundance dimension. In addition to the elements measured for DR14, an attempt was made to measure the abundance of cerium using a single line from Cunha et al. (2017), but these results show significant scatter and may be of limited utility.

In previous releases, we derived an internal calibration to the abundances to account for biases as a function of $T_{\rm eff}$, but for DR16 no such calibration is applied because, with the modification to the abundance pipeline, the trends with effective temperature for most elements have reduced amplitude as compared with previous data processing. The zero-point scale of the abundances was adjusted so that stars in the solar neighborhood (within 0.5 kpc of the Sun, according to Gaia parallaxes) with near-solar metallicity ($-0.05 >$ [M/H] < 0.05) are adjusted to have a mean [X/M] = 0. The reason for this choice is discussed in detail in Jönsson et al. (2020).

The procedure is described in significantly more detail, along with an assessment of the quality of the stellar parameters and abundances, in Jönsson et al. (2020).

4.4. Data Quality

The quality of the DR16 results for radial velocities, stellar parameters, and abundances is similar to that of previous APOGEE data releases. Figure 3 shows a $T_{\rm eff}$–log g diagram for the main sample APOGEE stars in DR16. The use of MARCS atmosphere models (Gustafsson et al. 2008) across the entire $T_{\rm eff}$–log g range has significantly improved results for cooler giants; previously, Kurucz atmosphere models (Castelli & Kurucz 2003) were used for the latter stars, and discontinuities were visible at the transition point between MARCS and Kurucz. While the stellar parameters are overall an improvement from previous DRs, we still apply external calibrations to both log g and $T_{\rm eff}$. These calibrations are discussed fully in Jönsson et al. (2020), who also describe the features in Figure 3 in more detail.

Several fields were observed with both the APOGEE-N and APOGEE-S instruments. Comparing the results, we find close agreement in the derived stellar parameters and abundances, with mean offsets of $\Delta T_{\rm eff} \sim 10$ K, $\Delta \log g \sim 0.02$ dex, and abundance offsets of <0.02 dex for most elements.

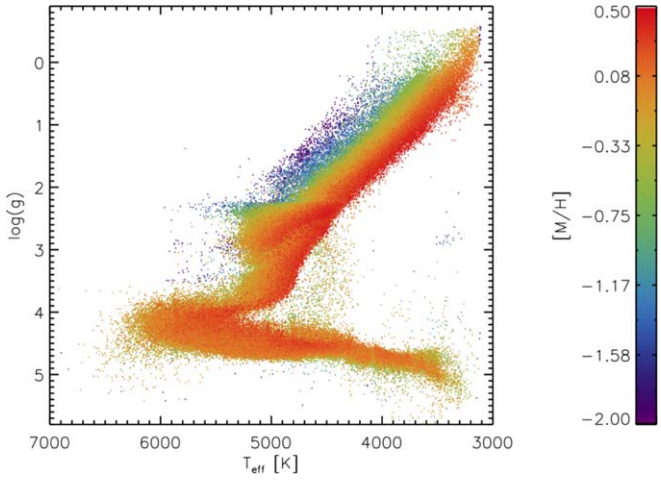

Figure 3. Spectroscopic Hertzsprung–Russell diagram, $T_{\rm eff}$ vs. log g for the main red star sample in APOGEE DR16. The points are color-coded by their total metal content, [M/H]. Dwarf-type stars, those with log $g > 3.7$ dex, have calibrated stellar parameters for the first time in DR16. New stellar grids also provide reliable measurements to cooler temperatures than in previous DRs.

4.5. APOGEE VACs

There are six APOGEE-associated VAC's in DR16. A brief description of each VAC and the corresponding publications are given below. They are also listed in Table 2.

4.5.1. APOGEE Red Clump Catalog

DR16 contains the latest version of the APOGEE red-clump (APOGEE-RC) catalog. This catalog is created in the same way as the DR14 version (which is presented in Bovy et al. 2014), with the more stringent log g cut. The DR16 catalog contains 39,675 unique stars, about 30% more than in DR14. The red clump stars are cross-matched to Gaia DR2 (Gaia Collaboration et al. 2018) by matching (R.A., decl.) within a radius of 2″ using the Vizier xmatch service.[147] We include proper motions (PMs) through this match.

4.5.2. APOGEE-astroNN

The APOGEE-astroNN VAC contains the results from applying the astroNN deep-learning code to APOGEE spectra to determine stellar parameters, individual stellar abundances (Leung & Bovy 2019a), distances (Leung & Bovy 2019b), and ages (Mackereth et al. 2019). Full details of how all of these quantities are determined from the DR16 data are given in Section 2.1 of Bovy et al. (2019). In addition, properties of the orbits in the Milky Way (and their uncertainties) for all stars are computed using the fast method of Mackereth & Bovy (2018) assuming the MWPotential2014 gravitational potential from Bovy (2015). Typical uncertainties in the parameters are 60 K in $T_{\rm eff}$, 0.2 dex in log g, 0.05 dex in elemental abundances, 5 % in distance, and 30 % in age. Orbital properties such as the eccentricity, maximum height above the mid-plane, radial, and vertical action are typically precise to 4%–8%.

[146] https://github.com/callendeprieto/ferre

[147] accessed through the gaia_tools code available here: https://github.com/jobovy/gaia_tools.

4.5.3. *APOGEE*-Joker

The APOGEE-*Joker* VAC contains posterior samplings over binary star orbital parameters (i.e., Keplerian orbital elements) for 224,401 stars with three or more APOGEE visit spectra that pass a set of quality cuts as described in Price-Whelan et al. 2020). The samplings are generated using *The Joker*, a custom Monte Carlo sampler designed to handle the very multi-modal likelihood functions that are natural to sparsely sampled or noisy RV time series (Price-Whelan et al. 2017, 2018). For some stars, these samplings are unimodal in period, meaning that the data are very constraining and the orbital parameters can be uniquely summarized; in these cases, we provide summary information about the samplings such as the maximum a posteriori sample values.

Price-Whelan et al. (2020) describes the resulting catalog from applying of *The Joker* to APOGEE DR16. Based on some simple cuts comparing the maximum likelihood posterior sample to the likelihood of a model for each source in which the radial velocities are constant (both quantities are provided in the VAC metadata), we estimate that there are $\gtrsim$25,000 binary star systems robustly detected by APOGEE (described in Price-Whelan et al. 2020, their Section 5). The vast majority of these systems have very poorly constrained orbital parameters, but these posterior samplings are still useful for performing hierarchical modeling of the binary star population parameters (e.g., period distribution and eccentricity parameters) as is demonstrated in Price-Whelan et al. (2020).

While finalizing the DR16 VAC release, we found a bug in the version of *The Joker* that was used to generate the posterior samplings released in this VAC. This bug primarily impacts long-period orbital parameter samplings, and only for systems with RV measurements that are very noisy or have a short baseline relative to the periods of interest. The samplings for systems with precise data or with many epochs should not be affected. Price-Whelan et al. (2020) describe the this bug in more detail. The VAC will be updated as soon as possible.

4.5.4. *Open Cluster Chemical Abundances and Mapping*

The goal of the Open Cluster Chemical Abundances and Mapping (OCCAM) survey is to create a uniform (same spectrograph, same analysis pipeline) open cluster abundances data set. We combine PM and RV measurements from Gaia DR2 (Gaia Collaboration et al. 2018) with RV and metallicity measurements from APOGEE to establish membership probabilities for each star observed by APOGEE in the vicinity of an open cluster. DR16 is the second VAC from the OCCAM survey. We do not impose a minimum number of reliable member stars as in the previous version (released in DR15, Aguado et al. 2019, and described in detail in Donor et al. 2018), but we do enforce a visual quality cut based on each cluster's PM-cleaned color–magnitude diagram. A detailed description of the updated methods is provided in Donor et al. (2020). The VAC includes 10,191 APOGEE stars in the vicinity of 126 open clusters. Average RV, PM, and abundances for reliable ASPCAP elements are provided for each cluster, along with the visual quality determination. Membership probabilities based individually upon RV, PM, and [Fe/H] are provided for each star. The reported cluster PM is from the kernel-smoothing routine used to determine cluster membership. Reported RVs and chemical abundances are simply the average value from cluster members; in practice, the uncertainties for chemical abundances are small and show small variation between stars of the same cluster.

4.5.5. *APOGEE DR16 StarHorse Distances and Extinctions*

The APOGEE DR16 StarHorse catalog contains updated distance and extinction estimates obtained with the latest version of the StarHorse code (Queiroz et al. 2018; Anders et al. 2019). The DR14 version of these results were published as part of the APOGEE DR14 Distance VAC (Abolfathi et al. 2018; Section 5.4.3). DR16 results are reported for 388,815 unique stars, based on the following input data: APOGEE DR16 ASPCAP results, broadband photometry from several sources (PanSTARRS-1, Two Micron All Sky Survey, AllWISE), as well as parallaxes from Gaia DR2 corrected for the zero-point offset of −0.05 mas found by Zinn et al. (2019). Typical statistical distance uncertainties amount to 10% for giant stars and 3% for dwarfs, respectively. Extinction uncertainties amount to 0.07 mag for stars with optical photometry and 0.17 mag for stars with only infrared photometry. The APOGEE DR16 StarHorse results are presented in Queiroz et al. (2020), together with updated results derived using spectroscopic information from other surveys.

5. eBOSS: Final Sample Release

Observations for eBOSS were conducted with the 1000-fiber BOSS spectrograph (Smee et al. 2013) to measure the distance–redshift relation with the baryon acoustic oscillation (BAO) feature that appears at a scale of roughly 150 Mpc. The last observations that will contribute to LSS measurements concluded on 2019 March 1. All eBOSS observations were conducted simultaneously with either TDSS observations of variable sources or SPIDERS observations of X-ray sources.

5.1. *eBOSS*

The first generation of the SDSS produced a spectroscopic LRG sample (Eisenstein et al. 2001) that led to a detection of the BAO feature in the clustering of matter (Eisenstein et al. 2005) and the motivation for dedicated LSS surveys within the SDSS. Over the period 2009–2014, BOSS completed a BAO program using more than 1.5 million galaxy spectra spanning redshifts $0.15 < z < 0.75$ and more than 150,000 quasars at $z > 2.1$ that illuminate the matter density field through the Lyα forest. Operating over the period 2014–2019, eBOSS is the third and final in the series of SDSS LSS surveys.

The eBOSS survey was designed to obtain spectra of four distinct target classes to trace the underlying matter density field over an interval in cosmic history that was largely unexplored during BOSS. The LRG sample covers the lowest-redshift interval within eBOSS, providing an expansion of the high-redshift tail of the BOSS galaxy sample (Reid et al. 2016) to a median redshift $z = 0.72$. Galaxy targets (Prakash et al. 2016) were selected from imaging catalogs derived from Wide-field Infrared Survey Explorer (WISE; Wright et al. 2010) and SDSS DR13 imaging data. A new sample of ELG targets covering $0.6 < z < 1.1$ was observed over the period 2016–2018, leading to the highest-redshift galaxy sample from the SDSS. Galaxy targets were identified using imaging from the Dark Energy Camera (DECam; Flaugher et al. 2015). The ELG selection (Raichoor et al. 2017) reaches a median redshift $z = 0.85$ and represents the first application of the DECam Legacy Survey data (DECaLS; Dey et al. 2019) to spectroscopic target selection in any large clustering survey. The

Table 3
Main Target Samples in eBOSS and BOSS

Sample	Redshift Range[a]	Number
eBOSS LRGs	$0.6 < z < 1.0$	298762
eBOSS ELGs	$0.6 < z < 1.1$	269889
eBOSS QSOs	$0.8 < z < 2.2$	434820
BOSS "LOWZ"[b]	$0.15 < z < 0.43$	343160
BOSS CMASS[c]	$0.43 < z < 0.75$	862735
BOSS Lyα QSOs	$2.2 < z < 3.5$	158917

Notes.
[a] Range used in clustering analysis
[b] The low redshift targets in BOSS
[c] "Constant mass" targets in BOSS

quasar sample covers the critical redshift range $0.8 < z < 2.2$ and is derived from WISE infrared and SDSS optical imaging data (Myers et al. 2015). Finally, new spectra of $z > 2.1$ quasars were obtained to enhance the final BOSS Lyα forest measurements (Bautista et al. 2017; du Mas des Bourboux et al. 2017). A summary of all these target categories, with redshift ranges and numbers, is provided in Table 3.

The surface area and target densities of each sample were chosen to maximize sensitivity to the clustering of matter at the BAO scale. The first major clustering result from eBOSS originated from the two year DR14 quasar sample. Using 147,000 quasars, a measurement of the spherically averaged BAO distance at an effective redshift $z = 1.52$ was performed with 4.4% precision (Ata et al. 2018). The DR14 LRG sample was used successfully to measure the BAO distance scale at 2.6% precision (Bautista et al. 2018) while the DR14 high-redshift quasar sample led to improved measurements of BAO in the auto-correlation of the Lyα forest (de Sainte Agathe et al. 2019) and the cross-correlation of the Lyα forest with quasars (Blomqvist et al. 2019). The DR14 samples have also been used to perform measurements of redshift–space distortions (RSD) (e.g., Zarrouk et al. 2018), tests of inflation (e.g., Castorina et al. 2019), and new constraints on the amplitude of matter fluctuations and the scalar spectral index (e.g., Chabanier et al. 2019).

5.1.1. Scope of eBOSS

With the completion of eBOSS, the BOSS and eBOSS samples provide six distinct target samples covering the redshift range $0.2 < z < 3.5$. The number of targets for each sample is summarized in Table 3 and the surface density of each sample is shown in Figure 4.

Figure 5 shows the DR16 eBOSS spectroscopic coverage in equatorial coordinates. For comparison, the SDSS-III BOSS coverage is shown in gray. The programs that define the unique eBOSS clustering samples are SEQUELS (Sloan Extended Quasar, ELG, and LRG Survey; initiated during SDSS-III; LRG and quasars), eBOSS LRG+QSO (the primary program in SDSS-IV observing LRGs and quasars or quasi-stellar objects (QSOs)), and ELG (new to DR16).

5.1.2. Changes to the eBOSS Spectral Reduction Algorithms

The data in DR16 were processed with version `v5_13_0` of the pipeline software `idlspec2d` (Bolton et al. 2012; Dawson et al. 2013). This is the last official version of the software that will be used for studies of LSS with the SDSS telescope. Table 4 presents a summary of the major changes in the pipeline during SDSS-IV (eBOSS) and we document the final changes to `idlspec2d` below.

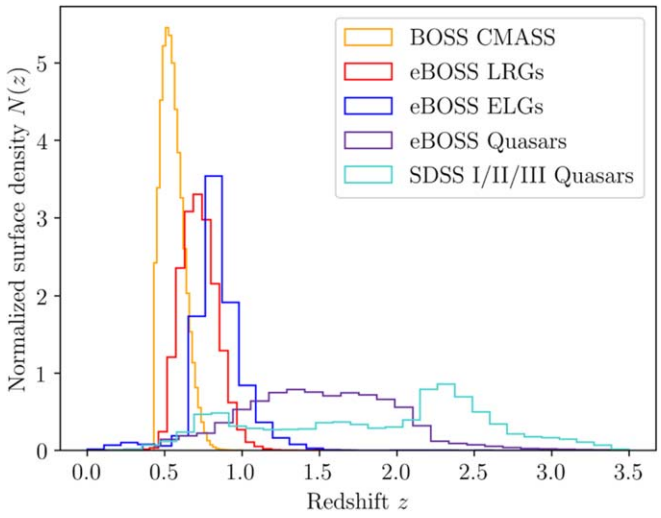

Figure 4. Normalized surface density ($N(z)$) of the spectroscopically confirmed objects used in the BOSS and eBOSS clustering programs. The SDSS-I,-II, and -III sample of confirmed quasars is also presented to demonstrate the gains in the number of quasars that eBOSS produced over the interval $0.8 < z < 2.2$.

There were two major changes from DR14 to DR16 to the reduction algorithm. First, a new set of stellar templates was used for the flux calibration. This set of templates was produced for the Dark Energy Spectroscopic Instrument (DESI) pipeline and provided to eBOSS. These templates reduce residuals in flux calibration relative to previous releases through improved modeling of spectral lines in the F-stars. The second major change was in the extraction step, where the background flux is now fitted prior to the extraction of the flux of individual traces. This modification improved the stability of extraction and removed occasional artifacts observed in low-S/N spectra. While these changes did not measurably improve the spectroscopic classification success rates, they represent an improvement in the overall data quality.

5.1.3. eBOSS VACs

There are two VACs based on eBOSS data which we release in DR16. These catalogs offer insight into galaxy physics with eBOSS spectra beyond the core cosmological goals. The catalogs are described below.

1. *Classification eBOSS ELGs*. This catalog gives the classification of $0.32 < z < 0.8$ eBOSS ELGs into four types: star-forming galaxies, composites, AGNs and low-ionization nuclear emission-line regions. It also contains the parameters: [O III]/Hβ, [O II]/Hβ, [O III] line velocity dispersion, and stellar velocity dispersion, $u - g$, $g - r$, $r - i$, $i - z$, which are used for classification. The classification is based on a random forest model trained using $z < 0.32$ ELGs labeled using standard optical diagnostic diagrams (Zhang et al. 2019). The codes, data, and data models are available at https://github.com/zkdtc/MLC_ELGs in addition to the standard location for VACs (see Section 3).
2. *FIREFLY Stellar Population Models of SDSS Galaxy Spectra (single fiber)*. We determine the stellar population properties (age, metallicity, dust reddening, stellar

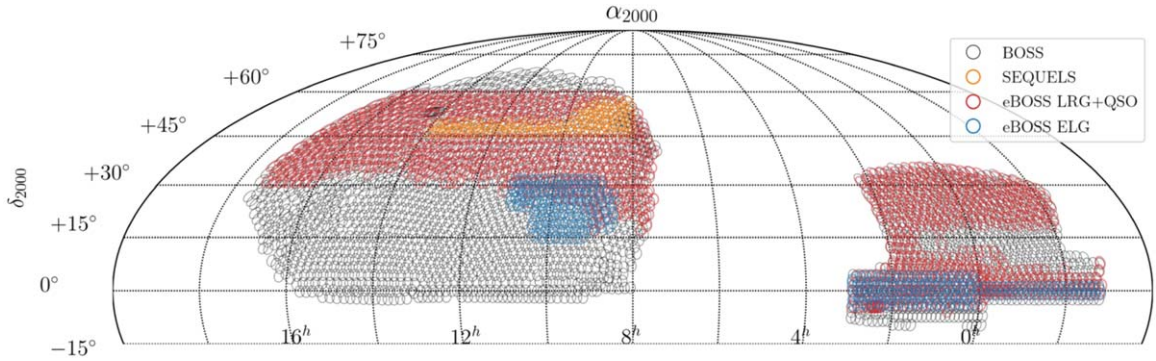

Figure 5. DR16 eBOSS spectroscopic coverage in equatorial coordinates (map centered at R.A. = 8h˙r.) Each symbol represents the location of a completed spectroscopic plate scaled to the approximate field of view. SPIDERS-maximal footprint is the same as BOSS, and SPIDERS-complete is SEQUELS. For more details on SPIDERS coverage see Comparat et al. (2020).

Table 4
Spectroscopic Pipeline Major Changes

Data Release	`idlspec2d` version	Major changes
DR12	`v5_7_0`	Final SDSS-III/BOSS release
DR13	`v5_9_0`	Adapting software to SDSS-IV/eBOSS data, new unbiased extraction algorithm
DR14	`v5_10_0`	New unbiased flux correction algorithm, ADR[a] corrections on individual exposures
DR16	`v5_13_0`	Improved background fitting in extraction, new stellar templates for flux calibration

Note.
[a] Atmospheric differential refraction.

mass, and star formation history (SFH)) for all single-fiber spectra classified as galaxies that were published in this release (including those from SDSS-I, -II, -III, and -IV). This catalog contains the newly completed samples of eBOSS LRGs and eBOSS ELGs and will be useful for a variety of studies on galaxy evolution and cosmology (e.g., Bates et al. 2019). This is an update of the calculation done by Comparat et al. (2017) on the galaxy spectra in DR14 (Abolfathi et al. 2018). We perform full spectral fitting on individual galaxy spectra using the FIREFLY[148] code (Wilkinson et al. 2015, 2017; Goddard et al. 2017a, 2017b) which make use of high spectral resolution stellar population models from Maraston and Strömbäck (2011). Calculations are carried out using the Chabrier (2003) stellar initial mass function and two input stellar libraries MILES and ELODIE (Sánchez-Blázquez et al. 2006; Prugniel et al. 2007; Falcón-Barroso et al. 2011). We publish all catalogs of properties through the SDSS web interfaces (SAS and CAS, see Section 3) and also make individual best-fit model spectra available through the FIREFLY website.[149]

In the future, we will also present a catalog of more than 800 candidate strong galaxy gravitational lens systems discovered by the presence of higher-redshift background emission lines in eBOSS galaxy spectra (M. Talbot et al. 2020, in preparation). This Spectroscopic Identification of Lensing Object (SILO; Talbot et al. 2018) program extends the method of the BOSS Emission-Line Lens Survey (Brownstein et al. 2012) and Sloan Lens ACS (Bolton et al. 2006) survey to higher redshift, and has recently been applied to the spectroscopic discovery of strongly lensed galaxies in MaNGA. The catalog will be released after DR16, but will be based on the DR16 sample.

5.1.4. Anticipated Cosmology Results from eBOSS

The final eBOSS BAO and RSD measurements will be presented in a series of independent analyses for each target class. The measurements performed with LRG, ELG, and $z < 2.2$ quasars will be performed in configuration space and Fourier space. Systematic errors will be assessed through the use of large N-body mock catalogs populated with galaxies according to a halo occupation distribution prescription that approximates the observed data, extending the work done in previous DRs (e.g., Gil-Marín et al. 2018). Consensus values of the angular diameter distance, the Hubble parameter, and $f\sigma_8$ will be provided for each tracer based on the two measurements. Measurements of the angular diameter distance and the Hubble parameter will be reported at $z > 2.1$ using both the auto-correlation of the final Lyα forest sample and the cross-correlation of the Lyα forest with quasars. All eBOSS results will be combined with the lower-redshift studies from SDSS and BOSS to offer new constraints on the cosmological model as was done in the DR11 sample for BOSS (Aubourg et al. 2015).

As part of the main cosmological goals of eBOSS, there will be a number of VACs based on the final eBOSS data released in DR16. VACs which are planned and will be publicly released in the future include the following.

1. *Large-scale Structure (from ELGs, LRGs, and QSOs).* These LSS VACs will be based on all available eBOSS data used for the clustering studies. Covering the main target classes, this VAC provides the tools to map the three-dimensional structure of the universe across $0.6 < z < 2.2$ (A. Ross et al. 2020, in preparation).

[148] https://github.com/FireflySpectra/firefly_release
[149] https://www.sdss.org/dr16/spectro/eboss-firefly-value-added-catalog/

2. *Lyα Forest Transmission VAC.* This VAC will contain the estimated fluctuations of transmitted flux fraction used for Lyα forest BAO measurements. The catalog will provide the estimates over the Lyα and Lyman-β rest frame regions of high-redshift quasars (H. du Mas des Bourboux 2020, in preparation).
3. *eBOSS Quasar Catalog.* Beginning with SDSS-I, the SDSS has maintained a tradition of releasing a visually inspected quasar catalog alongside major data releases. The new SDSS-DR16Q catalog (DR16Q; Lyke et al. 2020) will represent the most recent and largest catalog of known unique quasars within the SDSS.

5.2. RM Program and Other Repeat Spectroscopy

The SDSS-RM (Shen et al. 2015a) project is a dedicated multi-object RM program that began observations as a part of SDSS-III in 2014 January. Although not specifically established as a survey within eBOSS, observations of those same targets using the BOSS spectrograph continued through SDSS-IV. The SDSS-RM program monitors a sample of 849 quasars in a single $\sim$7 deg^2 pointing (observed with three plates, 7338, 7339, and 7340, with identical targets), with the overall goal of measuring black hole masses via RM in $\sim$100 quasars at a wide range of redshifts (details on the quasar sample itself are provided by Shen et al. 2019b). During the first season of SDSS-III monitoring, SDSS-RM obtained 32 epochs of SDSS spectroscopy, and has subsequently obtained $\sim$12 epochs yr^{-1} during 2015–2017 and $\sim$6 epochs yr^{-1} during 2018–2020 as part of SDSS-IV. The field has also been monitored photometrically with the Canada–France–Hawaii Telescope (CFHT) and the Steward Observatory Bok telescope in order to increase the observing cadence and the overall yield of RM time-lag measurements. The SDSS-RM field is also coincident with the Pan-STARRS 1 (PS1 Kaiser et al. 2010) Medium Deep Field MD07, and thus has been monitored photometrically since 2010. Observations with SDSS and the Bok telescope will continue through 2020.

The program has been largely successful in obtaining RM measurements: Shen et al. (2016b) reported several RM measurements from the program after analyzing the first year of spectroscopic data only, and Li et al. (2017) measured composite RM signals in the same data set. Grier et al. (2017) combined the first year of spectroscopy with the first year of photometry and recovered 44 lag measurements in the lowest-redshift subsample using the Hβ emission line. With the additional years of SDSS-IV monitoring included, Grier et al. (2019) reported 48 lag measurements using the CIV emission line; the addition of another year of SDSS spectroscopy and the inclusion of the PS1 photometric monitoring from 2010 to 2013 demonstrated the utility of longer time baselines in measuring additional lags (Shen et al. 2019a). Homayouni et al. (2019) measured inter-band continuum lags in many sources, allowing for investigations of accretion-disk properties. Additional studies based on SDSS-RM data that aim to evaluate and improve RM and black hole-mass measurement methodologies have also been completed (Li et al. 2019; Wang et al. 2019). The final SDSS-RM data set, which will make use of the PS1 monitoring of the SDSS-RM field and seven years of SDSS spectroscopic monitoring, will span more than 10 years and allow for the measurement of lags in the highest-luminosity subset of the quasar sample.

The SDSS-RM data set is extremely rich and allows for many other types of investigations beyond RM and black hole masses. The SDSS-RM group has also reported on many other topics, such as studies of quasar host galaxies (Matsuoka et al. 2015; Shen et al. 2015b; Yue et al. 2018), broad absorption-line (BAL) variability (Grier et al. 2015; Hemler et al. 2019), studies of extreme quasar variability (Dexter et al. 2019), and investigations of quasar emission-line properties (Sun et al. 2015, 2018; Denney et al. 2016a, 2016b; Shen et al. 2016a). RM observing will continue through 2020 at APO. Building on this program in SDSS-IV, an expanded multi-object spectroscopic RM program is included in the black hole mapper (BHM) program in the upcoming SDSS-V survey post-2020 (see Section 7).

In addition to the dedicated RM program, there were several fields in SDSS-III and SDSS-IV that were observed multiple times and thus offer similar potential for time-domain spectroscopic analyses. Those fields with at least four observations are as follows.

1. *Plates 3615 and 3647:* contain the standard BOSS selection of targets. These two plates have identical science targets and contain 14 epochs that are classified as "good" observations during SDSS-III.
2. *Plate 6782:* contains targets selected to be likely quasars based on variability from multi-epoch imaging data in Stripe 82 (York et al. 2000; Ivezić et al. 2007).[150] This plate contains four epochs that are classified as "good" observations during SDSS-III.
3. *Plates 7691 and 10000:* contain a standard eBOSS selection of LRG, quasar, SPIDERS, and TDSS targets. The two plates have identical selections and were observed nine times during SDSS-IV.
4. *Plate 9414:* contains ELG targets and TDSS targets from Stripe 82 and was observed four times to develop higher-S/N spectra that could be used to test the automated redshift classification schemes.

These multi-epoch fields and a few others from BOSS are described in more detail on the DR16 "Special Plates" website (https://sdss.org/dr16/spectro/special_plates/).

5.3. SPIDERS

SPIDERS is one of two smaller programs conducted within eBOSS. SPIDERS was originally designed as a multi-purpose follow-up program of the Spectrum-Roentgen-Gamma (SRG)/eROSITA all-sky survey (Merloni et al. 2012; Predehl et al. 2016), with the main focus on X-ray-selected AGNs and clusters of galaxies. Given the delay in the launch of SRG (which took place in 2019 July, i.e., after the end of the main eBOSS survey observing) the program was re-purposed to target the X-ray sources from the ROSAT All-Sky Survey (RASS; Voges et al. 1999, 2000) and XMM-Newton (X-ray Multi-mirror Mission; Jansen et al. 2001), which will be eventually have their X-ray emission better characterized by eROSITA.

All SPIDERS spectra taken since the beginning of SDSS-IV have targeted either X-ray sources from the revised data reduction of ROSAT (RASS, 2RXS; Voges et al. 1999, 2000; Boller et al. 2016) and XMM-Slew (Saxton et al. 2008)

[150] Also see https://classic.sdss.org/dr7/coverage/sndr7.html for details on Stripe 82 multi-epoch imaging.

catalogs, or red-sequence galaxies in clusters detected by ROSAT (part of the CODEX catalog; Finoguenov et al. 2020) or by XMM (XClass catalog; Clerc et al. 2012). We define two areas: "SPIDERS-Maximal" which corresponds to the sky area covered by an SDSS legacy or BOSS/eBOSS/SEQUELS plate, and "SPIDERS-Complete" which corresponds to the area covered by the eBOSS main survey and SEQUELS good plates. SPIDERS-Maximal (Complete) sky area amounts to 10,800 (5350) $\deg^2$. The sky area corresponding to SPIDERS-Complete is shown in Figure 5.

5.3.1. SPIDERS Clusters

In this section we describe the DR16 target selection, data scope, and VACs related to X-ray clusters. In DR16, 2740 X-ray-selected clusters (out of a total of 4114) were spectroscopically confirmed by SPIDERS observing over the SPIDERS-Complete area. This constitutes the largest X-ray cluster spectroscopic sample ever built. It forms the basis of multiple studies of structure formation on cosmological times (Furnell et al. 2018; Erfanianfar et al. 2019).

The majority of SPIDERS clusters targets are galaxies selected via the red-sequence technique around candidate X-ray galaxy clusters (Rykoff et al. 2012, 2014). These systems were found by filtering X-ray photon over-densities in RASS with an optical cluster finder tool using SDSS photometry. The target selection process for these targets is described fully in Clerc et al. (2016). The corresponding target bits and target classes are fully described in the SDSS DR14 data release (Abolfathi et al. 2018). We have also considered several additional SPIDERS cluster target classes which we describe below.

5.3.2. SPIDERS Target Selection Update

New for DR16 is data from "chunk `eboss20,26,27`." In chunk 20, `SPIDERS_RASS_CLUS` targets are obtained by extending the red-sequence search up to five times the cluster virial radius in CODEX clusters detected through their weak-lensing signature (Shan et al. 2014). The virial radius used in the target selection is provided in the value-added catalog. Moreover, in chunks 26 and 27, we introduce three new target subclasses, taking advantage of deeper optical data sets that enable cluster member measurements at higher redshifts.

1. `SPIDERS_CODEX_CLUS_CFHT`. Following the procedure described in Brimioulle et al. (2013), pointed CFHT/Megacam observations and CFHT-LS fields provide deep (*u*)*griz* photometry. A total of 54 (out of 462 targets) spectra were acquired and labeled with the bit mask `EBOSS_TARGET2` = 2^6;
2. `SPIDERS_CODEX_CLUS_PS1`. A sample of 249 high-redshift ($z_\lambda > 0.5$) CODEX cluster candidates were searched for red-sequence counterparts in Pan-STARRS PS1 (Flewelling et al. 2016) using a custom algorithm. A total of 129 (out of 1142 targets) spectra were acquired, and labeled with the bit mask `EBOSS_TARGET2` = 2^7;
3. `SPIDERS_CODEX_CLUS_DECALS`. These targets are output of a custom red-sequence finder code applied to DECaLS photometric data[151] (5th data release; Dey et al. 2019). A total of 48 spectra (out of 495 targets) were acquired and labeled with the bit mask `EBOSS_TARGET2` = 2^8.

[151] http://legacysurvey.org/decamls/

5.3.3. SPIDERS Galaxies and Redshifts

In the SPIDERS-Complete area, a total of 48,013 galaxy redshifts (observed by SDSS-I to -IV) are matched to red-sequence galaxy targets, regardless of any actual membership determination (Clerc et al. 2020) Of those, 26,527 are SPIDERS targets specifically. The additional redshifts were collected from past SDSS-I, -II, -III, and other eBOSS programs. The median *i*-band magnitudes of the 26,527 newly acquired targets are $i_{\rm fiber2} = 20.0$ and $i_{\rm cModel} = 18.5$. The spectra are typical of red, passive galaxies at $0.05 \lesssim z \lesssim 0.7$, displaying characteristic absorption features (Ca H+K, *G*-band, Mg I, NaD, etc.). Such magnitude and redshift ranges and the purposely narrow spectral diversity make the automated galaxy redshift determination a straightforward task for the eBOSS pipeline, which is well-optimized in this area of the parameter space (Bolton et al. 2012). In total, 47,492 redshifts are successfully determined with a `ZWARNING_NOQSO=0`. The remaining (∼1%) showing a non-zero flag are mainly due to due to unplugged fibers or bad columns on the spectrograph CCD or very low S/N; their redshift is not measured. Full details on the statistical properties of the sample, and in particular the success of redshift determination, are given in C. Kirkpatrick et al. (2020, in preparation).

5.3.4. VAC: SPIDERS X-Ray Clusters Catalog for DR16

Within the SPIDERS-Complete area, 2740 X-ray clusters showing a richness $\lambda_{\rm OPT} > 10$ were spectroscopically validated based on galaxy redshift data from SDSS-I to -IV in their red-sequence. The richness, $\lambda_{\rm OPT}$, is defined as the sum of the membership probability of every galaxy in the cluster field. It was measured by the redmapper algorithm (Rykoff et al. 2012). A total of 32,326 valid redshifts were associated with these galaxy clusters, leading to a median number of 10 redshifts per cluster red-sequence. The process of this validation is a combination of automatic and manual evaluations (C. Kirkpatrick et al. 2020, in preparation). An automated algorithm performed a preliminary membership assignment and interloper removal based on standard iterative σ-clipping methods. The results of the algorithm were visually inspected by six experienced galaxy cluster observers (11 different people since the beginning of the survey), ensuring at least two independent inspectors per system. A web-based interface was specifically developed for this purpose: using as a starting point the result of the automated algorithm, the tool allows each inspector to interactively assess membership based on high-level diagnostics and figures (see Figure 16 in Clerc et al. 2016). Validation is in most cases a consequence of finding three or more red-sequence galaxies in a narrow redshift window all within the X-ray estimated viral radius, compatible with them all being galaxy cluster members. A robust weighted average of the cluster member redshifts provides the cluster systemic redshift.

5.3.5. X-Ray Pointlike Sources

Throughout SDSS-IV, the SPIDERS program has been providing spectroscopic observations of ROSAT/RASS and XMMSL1 sources in the BOSS footprint (Dwelly et al. 2017). In addition to those targeted by SPIDERS, a large number of ROSAT and XMMSL1 sources received spectra during the SDSS-I/II (in 2000–2008; York et al. 2000) and SDSS-III BOSS (in 2009–2014; Eisenstein et al. 2011; Dawson et al. 2013) surveys. By combining the SDSS-I to -IV spectra, the

spectroscopic completeness achieved for the ROSAT sample is $10{,}590/21{,}945 = 50\%$ in the SPIDERS-Complete area. It increases to 53% when considering only high-confidence X-ray detections, and to 95% when considering only sources with high-confidence X-ray detections and optical counterparts with magnitudes in the nominal eBOSS survey limits ($17 \leqslant i_{\mathtt{mFiber2}} \leqslant 22.5$). In the SPIDERS-Maximal area, the spectroscopic completeness of the ROSAT sample is lower, $17{,}300/40{,}929 = 42\%$ (45% and 62% respectively).

For ROSAT sources, the major difficulty lies in the identification of secure counterparts of the X-ray sources at optical wavelength, given the large positional uncertainties. To solve this problem, the Bayesian cross-matching algorithm NWAY (Salvato et al. 2018) was used. The priors for this were based on ALLWISE (Cutri et al. 2013) infrared color–magnitude distributions which, at the depth of the 2RXS and XMMSL2 surveys, can distinguish between X-ray-emitting and field sources. WISE positions were matched to photometric counterparts in the SDSS. So for the DR16 value-added catalogs, instead of reporting RASS of XMMSL1 measured X-ray fluxes, we report the updated 2RXS and XMMSL2 fluxes. Comparat et al. (2020) present the SPIDERS spectroscopic survey of X-ray pointlike sources, and a detailed description of the DR16 value-added catalogs. We summarize this below.

5.3.6. VACs: Multi-wavelength Properties of RASS and XMMSL AGNs

In these two VACs, we present the multiwavelength characterization over the SPIDERS-Complete area of two highly complete samples of X-ray sources.

1. The RASS X-ray source catalog (2RXS; Boller et al. 2016).
2. The XMM-Newton Slew Survey point source catalog (XMMSL2, Version 2; Saxton et al. 2008).

We provide information about the X-ray properties of the sources as well as of their counterparts at longer wavelengths (optical, infrared, and radio) identified first in the AllWISE Infrared catalog via a Bayesian cross-matching algorithm (Salvato et al. 2018). We complement this with dedicated visual inspection of all the SDSS spectra, providing accurate redshift estimates (with confidence levels based on the inspection) and source classification, beyond the standard eBOSS pipeline results. These two VACs supersede the two analogous ones published in DR14.

5.3.7. VAC: Spectral Properties and Black Hole Mass Estimates for SPIDERS DR16 Type 1 AGNs

This VAC contains optical spectral properties and black hole mass estimates for the DR16 sample of X-ray-selected SPIDERS type 1 (optically unobscured) AGNs. This is the DR16 edition of an earlier SPIDERS VAC covering SPIDERS type 1 AGNs up to DR14, which was presented by Coffey et al. (2019) and Aguado et al. (2019). The spectral regions around the Mg II and Hβ emission lines were fit using a multi-component model in order to derive optical spectroscopic properties as well as derive quantities such as black hole mass estimates and Eddington ratios.

5.3.8. Future Plans for SPIDERS

In addition to these programs, completed and fully released in DR16, the performance verification data being taken as part of the eROSITA Final Equatorial Field Depth Survey are currently planned to be available by November 2019 and should consist of 120 deg^2 observed to the final eROSITA all-sky survey depth over an equatorial field overlapping with the GAMA09 (Robotham et al. 2011) survey window. To address at least part of the original goals of SPIDERS (i.e., eROSITA follow-up) within SDSS-IV, we plan to dedicate a special set of 12 special plates for these targets, to be observed in spring 2020, and released as part of the final 17th DR. An extensive eROSITA follow-up program is also planned for the next generation of the survey, SDSS-V (Kollmeier et al. 2017, and see Section 7) and 4MOST (Finoguenov et al. 2019; Merloni et al. 2019).

5.4. TDSS

TDSS is the second large subprogram of eBOSS, the goal of which is to provide the first large-scale, systematic survey of spectroscopic follow-up to characterize photometric variables. TDSS makes use of the BOSS spectrographs (Smee et al. 2013), using a small fraction (about 5%) of the optical fibers on eBOSS plates. TDSS observations thus concluded with the end of the main eBOSS survey data collection 2019 March 1, and the full and final TDSS spectroscopic data are included in DR16.

There are three main components of TDSS, each now with data collection complete.

1. The primary TDSS spectroscopic targets are selected from their variability within Pan-STARRS1 (PS1 multi-epoch imaging photometry, and/or from longer-term photometric variability between PS1 and SDSS imaging data; see, e.g., Morganson et al. 2015). TDSS single-epoch spectroscopy (Ruan et al. 2016) of these targets establishes the nature of the photometric variable (e.g., variable star versus variable quasar, and subclass, etc.), and in turn often then suggests the character of the underlying variability (e.g., pulsating RR Lyrae versus flaring late-type star versus cataclysmic variable, etc.). More than 108,000 optical spectra of these TDSS photometric variables have been observed through DR16 (in both eBOSS and the eBOSS pilot program SEQUELS). Adding in similar variables sources fortuitously already having optical spectra within the SDSS archives (from SDSS-I, -II, or -III), approximately one-third of the TDSS variables can be spectroscopically classified as variable stars, and the majority of the remaining two-thirds are variable quasars.
2. A sample of 6500 TDSS spectroscopic fibers were allotted to obtain repeat spectra of known star and quasar subclasses of unusual and special interest, which were anticipated or suspected to exhibit spectroscopic variability in few-epoch spectroscopy (FES; see e.g., MacLeod et al. 2018). A recent specific example of this category of sources are TDSS spectra of nearly 250 dwarf carbon stars that provide strong evidence of statistical RV variations indicative of subclass binarity (Roulston et al. 2019).
3. The more recently initiated TDSS Repeat Quasar Spectroscopy (RQS) program (see MacLeod et al. 2018) obtains

multi-epoch spectra for 16,500 known quasars, sampling across a broad range of properties including redshift, luminosity, and quasar subclass type. This has a larger sample size, and also a greater homogeneity and less a priori bias to specific quasar subclasses compared to the TDSS FES program. All RQS targets have at least one earlier epoch of SDSS spectroscopy already available in the SDSS archive. The RQS program is designed especially to investigate quasar spectral variability on multi-year timescales and, in addition to its own potential for new discoveries of phenomena such as changing-look quasars or BAL variability and others, also provides a valuable (and timely) resource for planning of yet larger-scale multi-epoch quasar repeat spectral observations anticipated for the SDSS-V BHM program (see Section 7).

In total, TDSS has selected or co-selected (in the latter case, often with eBOSS quasar candidate selections) more than 131,000 spectra in SDSS-IV that probe spectroscopy in the time domain. All of these spectra are now being released in DR16.

6. MaNGA: VACs Only

MaNGA continues to observe galaxies at APO and, following the end of eBOSS observing, now uses all dark time at APO. Technical papers are available which overview the project (Bundy et al. 2015), target selection (Wake et al. 2017), instrumentation (Drory et al. 2015), observing (Law et al. 2015; Yan et al. 2016a), and data reduction and calibration strategies (Law et al. 2016; Yan et al. 2016b). For DR16 there is no new data release of MaNGA data cubes or analysis products; all remaining data will be released in DR17. However, two new or updated MaNGA related VACs are provided, which we document here. Previously released VACs, which are still available, include those that provide stellar masses, morphologies, and neutral hydrogen (H I) followup (for details of DR15 VACs, see Aguado et al. 2019[152]).

6.1. Stellar Masses from Principal Component Analysis

This VAC provides measurements of resolved and total galaxy stellar masses, obtained from a low-dimensional fit to the stellar continuum: Pace et al. (2019a) document the method used to obtain the stellar continuum fit and measurements of resolved stellar mass-to-light ratio, and Pace et al. (2019b) address the aggregation into total galaxy stellar masses, including aperture-correction and accounting for foreground stars. The measurements rely on MaNGA DRP version `v2_5_3`, data analysis pipeline version `2.3.0`, and `PCAY` version `1.0.0`.[153] The VAC includes maps of stellar mass-to-light ratio and *i*-band luminosity (in solar units), a table of aperture-corrected total galaxy stellar masses, a library of synthetic model spectra, and the resulting low-dimensional basis set.

The low-dimensional basis set used to fit the stellar continuum is generated by performing principal component analysis (PCA) on a library of 40,000 synthetic SFHs: the SFHs are delayed-τ models (SFR $\sim t\, e^{-t/\tau}$) modulated by infrequent starbursts, sharp cutoffs, and slow rejuvenations (see Pace et al. 2019a, Section 3.1.1). Broad priors dictate the possible range in stellar metallicity, attenuation by foreground dust, and uncertain phases of stellar evolution such as blue stragglers and blue horizontal branch stars (see Pace et al. 2019a, Section 3.1.2). The system of six principal component spectra ("eigenspectra") is used as a low-dimensional basis set for fitting the stellar continuum. A distribution of stellar mass-to-light ratio is obtained for each MaNGA spaxel (line of sight in a galaxy) by weighting each model spectrum's known mass-to-light ratio by its likelihood given an observed spectrum. The median of that distribution is adopted as the fiducial stellar mass-to-light ratio of a spaxel, and multiplied by the *i*-band luminosity to get an estimate for the stellar mass.

For DR16, *i*-band stellar mass-to-light ratio and *i*-band luminosity maps (both in solar units) are released. Stellar mass-to-light ratios have been vetted against synthetic spectra, and found to be reliable at median S/Ns, from S/N = 2–20, across a wide range of dust attenuation conditions (optical depth in the range 0–4), and across the full range of realistic stellar metallicities (−2 to +0.2 dex), with respect to solar (see Pace et al. 2019a, Section 4.10). Typical "random" uncertainties are approximately 0.1 dex (including age–metallicity degeneracies and uncertainties induced by imperfect spectrophotometry), and systematic uncertainties induced by choice of training SFHs could be as high as 0.3 dex, but are believed to be closer to 0.1–0.15 dex (see Pace et al. 2019a, Sections 4.10 and 5).

In addition to resolved maps of stellar mass-to-light ratio and *i*-band luminosity, the VAC includes a catalog of total stellar masses for MaNGA DR16 galaxies. We provide the total mass inside the integral field unit (IFU; after interpolating over foreground stars and other unreliable measurements with the median of its eight nearest neighbors: see Pace et al. 2019b, Section 4). We also supply two aperture corrections intended to account for mass falling outside the spatial grasp of the IFU: the first adopts the median stellar mass-to-light ratio of the outermost 0.5 effective radii, and the second (recommended) adopts a mass-to-light ratio consistent with the $(g - r)$ color of the NSA flux minus the flux in the IFU (see Pace et al. 2019b, Section 4). A comparison of these total masses with those from the NASA-Sloan Atlas (NSA; Blanton et al. 2011) and MPA-JHU[154] catalog (Brinchmann et al. 2004) is shown in Figure 6.

6.2. PawlikMorph Catalog

This catalog provides the shape asymmetry, alongside other standard galaxy morphological related measurements (CAS, Gini, M20, curve of growth radii, and Sérsic fits), based on SDSS DR7 imaging (Abazajian et al. 2009) using the eight-connected structure detection algorithm described in Pawlik et al. (2016)[155] to define the edges of the galaxies. We make this available for all galaxies in the MaNGA DR15 release (Aguado et al. 2019). The algorithm is specifically designed to identify faint features in the outskirts of galaxies. In this version, stars are not masked prior to creating the eight-connected binary mask, therefore stars lying within the extended light of the galaxies cause incorrect measurements. More than 10% of objects with unusual measurements have been visually inspected using Marvin and SkyServer, and the `WARNINGFLAG` set to 1 for the fraction of these where a star or other problem is identified. Users should not use these

[152] DR15 VACs are found at: https://www.sdss.org/dr15/data_access/value-added-catalogs/.
[153] https://www.github.com/zpace/pcay
[154] Max Planck Institute for Astrophysics and the Johns Hopkins University.
[155] Available from https://github.com/SEDMORPH/PawlikMorph.

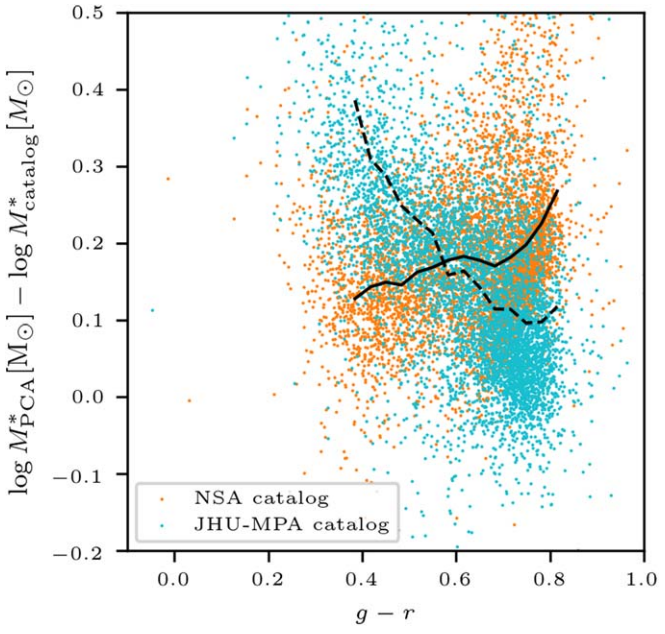

Figure 6. Comparison of MaNGA-PCA total stellar masses with NSA (blue points and dashed black line) and MPA-JHU (orange points and solid black line) stellar masses as a function of galaxy $g - r$ color. The lines show a locally weighted regression. This plot is reproduced from Figure 6 of Pace et al. (2019b).

measurements, and additionally may wish to visually inspect small samples or outliers to ensure that the sample is appropriate for their science goals.

7. Conclusions and Future Plans

This data release, which is the 16th overall from the SDSS (DR16), is notable for containing the first release of data from Southern Hemisphere observing as part of APOGEE-2S and the last release of large-scale cosmological redshift-survey data from the SDSS (the main program of the eBOSS survey). DR16 contains no new data from the MaNGA survey.

SDSS-IV has one final year of operations remaining, and is planning a further final public data release. That data release, which will be the 17th from SDSS overall (DR17), will comprise all remaining data taken by all surveys in SDSS-IV. What follows is a brief summary of the intended contents of DR17.

1. Due to an accelerated pace of observing in 2018 February–2019 March 1, eBOSS has finished observing, and so DR16 is the final data release for both the main eBOSS survey and TDSS. A number of catalogs of redshifts based on eBOSS DR16 spectra have been constructed; these will be released in the future. The successful launch of the eROSITA satellite (Predehl et al. 2014) means there will be a small number of additional SPIDERS plates for followup of eROSITA targets, the spectra from which will be released in DR17.
2. MaNGA has been observing in all remaining dark time from APO since 2019 March 2, and is on schedule to meet, or slightly exceed, its intended goal of 10,000 galaxies. In addition MaNGA has been approved time to observe a subset of ($N \sim 400$) galaxies at an exposure time four times deeper than the typical survey.
3. APOGEE-2 continues to observe from both the Northern (APO) and Southern (LCO) Hemisphere. DR16 is the first release of data from the Southern Hemisphere, and DR17 will be the final release of all APOGEE data from all phases of APOGEE. DR17 will have the complete multi-epoch samples spanning as long as 10 years for some targets, as well as reaching both full depth and coverage in the disk, bulge, and halo programs, and completing large-scale programs to characterize photometric objects of interest in Kepler, K2, and TESS.

7.1. SDSS-V

Starting in 2020, after SDSS-IV has ended observations at APO and LCO, the next generation of the SDSS will begin—SDSS-V (Kollmeier et al. 2017).[156] SDSS-V is a multi-epoch spectroscopic survey to observe nearly six million sources using the existing BOSS and APOGEE spectrographs, as well as very large swathes of interstellar medium (ISM) in the Local Group using new optical spectrographs and a suite of small telescopes. SDSS-V will operate at both APO and LCO, providing the first all-sky "panoptic" spectroscopic view of the sky, and will span a wide variety of target types and science goals.

The scientific program is divided into three "Mappers."

1. The *Milky Way Mapper* (MWM) is targeting millions of stars with the APOGEE and BOSS spectrographs, ranging from the immediate solar neighborhood to the far side of the Galactic disk and the Milky Way's satellite companions. The MWM will probe the formation and evolution of the Milky way, the physics and life-cycles of its stars, and the architecture of multi-star and planetary systems.
2. The *BHM* is targeting nearly half a million super-massive black holes and other X-ray sources (including newly discovered systems from the eROSITA mission) with the BOSS spectrograph in order to characterize the X-ray sky, measure black hole masses, and trace black hole growth across cosmic time.
3. Finally, the *Local Volume Mapper* (LVM) employs a wide-field optical IFU and new optical spectrographs (with $R \sim 4000$) to map $\sim$2500 deg^2 of sky, targeting the ISM and embedded stellar populations in the Milky Way and satellite galaxies. These maps will reveal the physics of both star formation and the interplay between these stars and the surrounding ISM.

SDSS-V builds upon the operational infrastructure and data legacy of earlier SDSS programs, with the inclusion of several key new developments. Among these are the retirement of the SDSS plug–plate system and the introduction of robotic fiber positioners in the focal planes of both 2.5 m telescopes at APO and LCO. These focal plane systems enable more efficient observing and larger target densities than achievable in previous SDSS surveys. In addition, the LVM is facilitated by the construction of several $\leqslant$1 m telescopes at one or both observatories, linked to several new optical spectrographs based on the DESI design (Martini et al. 2018). SDSS-V continues the SDSS legacy of open data policies and convenient, efficient public data access, with improved data

[156] https://www.sdss.org/future

distribution systems to serve its large, diverse, time-domain, multi-object, and integral-field data set to the world.

After 20 years of Sloan Digital Sky Surveys the data coming out from SDSS-IV in DR16 is making significant contributions to our understanding of the components our Galaxy, galaxy evolution in general, and the universe as a whole. The SDSS-IV project will end with the next data release (DR17), but the future is bright for SDSS with new technology and exciting new surveys coming in SDSS-V.

Funding for the Sloan Digital Sky Survey IV has been provided by the Alfred P. Sloan Foundation, the U.S. Department of Energy Office of Science, and the Participating Institutions. SDSS-IV acknowledges support and resources from the Center for High-Performance Computing at the University of Utah. The SDSS website is www.sdss.org.

SDSS-IV is managed by the Astrophysical Research Consortium for the Participating Institutions of the SDSS Collaboration including the Brazilian Participation Group, the Carnegie Institution for Science, Carnegie Mellon University, the Chilean Participation Group, the French Participation Group, Harvard-Smithsonian Center for Astrophysics, Instituto de Astrofísica de Canarias, The Johns Hopkins University, Kavli Institute for the Physics and Mathematics of the Universe (IPMU)/University of Tokyo, Korean Participation Group, Lawrence Berkeley National Laboratory, Leibniz Institut für Astrophysik Potsdam (AIP), Max-Planck-Institut für Astronomie (MPIA Heidelberg), Max-Planck-Institut für Astrophysik (MPA Garching), Max-Planck-Institut für Extraterrestrische Physik (MPE), National Astronomical Observatories of China, New Mexico State University, New York University, University of Notre Dame, Observatário Nacional/MCTI, The Ohio State University, Pennsylvania State University, Shanghai Astronomical Observatory, United Kingdom Participation Group, Universidad Nacional Autónoma de México, University of Arizona, University of Colorado Boulder, University of Oxford, University of Portsmouth, University of Utah, University of Virginia, University of Washington, University of Wisconsin, Vanderbilt University, and Yale University.

Co-authorship on SDSS-IV data papers is alphabetical by last name and offered to all collaboration members who have contributed at least one month FTE toward any of the surveys during the period up to the end of data collection; and any external collaboration who has contributed at least one month FTE to work critical to the data release.

We would like to thank the Center for Cosmology and AstroParticle Physics (CCAPP) at the Ohio State University for their hospitality during "DocuBrew" 2019. This event held in 2019 August was the main venue for documentation updates for DR16 (including this paper), was organized by A.R., J.J., and A.-M.W and attended by R.B., J.B., B.C., K.D., S.H., A.J., J.H., K.M., J.R., J.S.-G., F.S., and M.T. (and remotely by H.J., J.B., J.H., J.S., C.G. J.C., S.A., R.T., B.L., and J.P.). Figures 1 and 2 were made by C.H. Figure 4 was made by A.R. and Figure 5 by M.V. and J.B.

This research made use of ASTROPY, a community-developed core PYTHON (http://www.python.org) package for Astronomy (Robitaille et al. 2013), IPYTHON (Pérez & Granger 2007), MATPLOTLIB (Hunter 2007), NUMPY (Walt et al. 2011), SCIPY (Virtanen et al. 2020), and TOPCAT (Taylor 2005).

ORCID iDs

Brett H. Andrews https://orcid.org/0000-0001-8085-5890
Borja Anguiano https://orcid.org/0000-0001-5261-4336
Vladimir Avila-Reese https://orcid.org/0000-0002-3461-2342
Carles Badenes https://orcid.org/0000-0003-3494-343X
Kat Barger https://orcid.org/0000-0001-5817-0932
Jorge K. Barrera-Ballesteros https://orcid.org/0000-0003-2405-7258
Sarbani Basu https://orcid.org/0000-0002-6163-3472
Julian Bautista https://orcid.org/0000-0002-9885-3989
Rachael L. Beaton https://orcid.org/0000-0002-1691-8217
Timothy C. Beers https://orcid.org/0000-0003-4573-6233
Chad F. Bender https://orcid.org/0000-0003-4384-7220
Matthew Bershady https://orcid.org/0000-0002-3131-4374
Dmitry Bizyaev https://orcid.org/0000-0002-3601-133X
Michael R. Blanton https://orcid.org/0000-0003-1641-6222
Jura Borissova https://orcid.org/0000-0002-5936-7718
Jo Bovy https://orcid.org/0000-0001-6855-442X
W. N. Brandt https://orcid.org/0000-0002-0167-2453
Joel R. Brownstein https://orcid.org/0000-0002-8725-1069
Kevin Bundy https://orcid.org/0000-0001-9742-3138
Martin Bureau https://orcid.org/0000-0003-4980-1012
Adam Burgasser https://orcid.org/0000-0002-6523-9536
Michele Cappellari https://orcid.org/0000-0002-1283-8420
Ricardo Carrera https://orcid.org/0000-0001-6143-8151
William Chaplin https://orcid.org/0000-0002-5714-8618
Brian Cherinka https://orcid.org/0000-0002-4289-7923
S. Drew Chojnowski https://orcid.org/0000-0001-9984-0891
Haeun Chung https://orcid.org/0000-0002-3043-2555
Johan Comparat https://orcid.org/0000-0001-9200-1497
Kevin Covey https://orcid.org/0000-0001-6914-7797
Jeffrey D. Crane https://orcid.org/0000-0002-5226-787X
Katia Cunha https://orcid.org/0000-0001-6476-0576
Jeremy Darling https://orcid.org/0000-0003-2511-2060
Roger Davies https://orcid.org/0000-0001-7897-3812
Kyle Dawson https://orcid.org/0000-0002-0553-3805
Nathan De Lee https://orcid.org/0000-0002-3657-0705
Niv Drory https://orcid.org/0000-0002-7339-3170
Arthur Davis Eigenbrot https://orcid.org/0000-0003-0810-4368
Xiaohui Fan https://orcid.org/0000-0003-3310-0131
Diane Feuillet https://orcid.org/0000-0002-3101-5921
Alexis Finoguenov https://orcid.org/0000-0002-4606-5403
Peter M. Frinchaboy https://orcid.org/0000-0002-0740-8346
Hai Fu https://orcid.org/0000-0001-9608-6395
Lluís Galbany https://orcid.org/0000-0002-1296-6887
Rafael A. Garcia https://orcid.org/0000-0002-8854-3776
Doug Geisler https://orcid.org/0000-0002-3900-8208
Joseph Gelfand https://orcid.org/0000-0003-4679-1058
Julian Goddy https://orcid.org/0000-0002-8933-9574
Paul Green https://orcid.org/0000-0002-8179-9445
Catherine J. Grier https://orcid.org/0000-0001-9920-6057
Hong Guo https://orcid.org/0000-0003-4936-8247
Paul Harding https://orcid.org/0000-0003-3442-6248
Christian R. Hayes https://orcid.org/0000-0003-2969-2445
David W. Hogg https://orcid.org/0000-0003-2866-9403
Jon A. Holtzman https://orcid.org/0000-0002-9771-9622
Bau-Ching Hsieh https://orcid.org/0000-0001-5615-4904
Daniel Huber https://orcid.org/0000-0001-8832-4488

Jason A. S. Hunt https://orcid.org/0000-0001-8917-1532
Jennifer A. Johnson https://orcid.org/0000-0001-7258-1834
Eric Jullo https://orcid.org/0000-0002-9253-053X
Karen Kinemuchi https://orcid.org/0000-0001-7908-7724
Juna A. Kollmeier https://orcid.org/0000-0001-9852-1610
Marina Kounkel https://orcid.org/0000-0002-5365-1267
Dhanesh Krishnarao https://orcid.org/0000-0002-7955-7359
Ivan Lacerna https://orcid.org/0000-0002-7802-7356
Ting-Wen Lan https://orcid.org/0000-0001-8857-7020
David R. Law https://orcid.org/0000-0002-9402-186X
Hannah Lewis https://orcid.org/0000-0002-7871-085X
Jianhui Lian https://orcid.org/0000-0001-5258-1466
Britt Lundgren https://orcid.org/0000-0002-6463-2483
Brad W. Lyke https://orcid.org/0000-0002-5078-2472
Steven R. Majewski https://orcid.org/0000-0003-2025-3147
Arturo Manchado https://orcid.org/0000-0002-3011-686X
Paul Martini https://orcid.org/0000-0002-4279-4182
Karen L. Masters (何凱論) https://orcid.org/0000-0003-0846-9578
Savita Mathur https://orcid.org/0000-0002-0129-0316
Andrea Miglio https://orcid.org/0000-0001-5998-8533
Dante Minniti https://orcid.org/0000-0002-7064-099X
Takamitsu Miyaji https://orcid.org/0000-0002-7562-485X
Seshadri Nadathur https://orcid.org/0000-0001-9070-3102
Kirpal Nandra https://orcid.org/0000-0002-7150-9192
Rebecca Jean Nevin https://orcid.org/0000-0003-1056-8401
Jeffrey A. Newman https://orcid.org/0000-0001-8684-2222
David L. Nidever https://orcid.org/0000-0002-1793-3689
Christian Nitschelm https://orcid.org/0000-0003-4752-4365
Zachary J. Pace https://orcid.org/0000-0003-4843-4185
Nelson Padilla https://orcid.org/0000-0001-9850-9419
Nathalie Palanque-Delabrouille https://orcid.org/0000-0003-3188-784X
Hsi-An Pan https://orcid.org/0000-0002-1370-6964
Kaike Pan https://orcid.org/0000-0002-2835-2556
Will J. Percival https://orcid.org/0000-0002-0644-5727
Ismael Perez-Fournon https://orcid.org/0000-0002-2807-6459
Marc Pinsonneault https://orcid.org/0000-0002-7549-7766
Joshua Tyler Povick https://orcid.org/0000-0002-6553-7082
Abhishek Prakash https://orcid.org/0000-0003-4451-4444
Adrian M. Price-Whelan https://orcid.org/0000-0003-0872-7098
Rogemar A. Riffel https://orcid.org/0000-0003-0483-3723
Hans-Walter Rix https://orcid.org/0000-0003-4996-9069
Annie C. Robin https://orcid.org/0000-0001-8654-9499
A. Roman-Lopes https://orcid.org/0000-0002-1379-4204
Carlos Román-Zúñiga https://orcid.org/0000-0001-8600-4798
Benjamin Rose https://orcid.org/0000-0002-1873-8973
Ashley J. Ross https://orcid.org/0000-0002-7522-9083
Kate Rowlands https://orcid.org/0000-0001-7883-8434
Kate H. R. Rubin https://orcid.org/0000-0001-6248-1864
Mara Salvato https://orcid.org/0000-0001-7116-9303
Jaderson S. Schimoia https://orcid.org/0000-0002-5640-6697
Edward Schlafly https://orcid.org/0000-0002-3569-7421
David Schlegel https://orcid.org/0000-0002-5042-5088
Mathias Schultheis https://orcid.org/0000-0002-6590-1657
Hee-Jong Seo https://orcid.org/0000-0002-6588-3508
Arman Shafieloo https://orcid.org/0000-0001-6815-0337
Shiyin Shen https://orcid.org/0000-0002-3073-5871
Matthew Shetrone https://orcid.org/0000-0003-0509-2656
Anže Slosar https://orcid.org/0000-0002-8713-3695
Jennifer Sobeck https://orcid.org/0000-0002-4989-0353
Diogo Souto https://orcid.org/0000-0002-7883-5425
David V. Stark https://orcid.org/0000-0002-3746-2853
Keivan G. Stassun https://orcid.org/0000-0002-3481-9052
Matthias Steinmetz https://orcid.org/0000-0001-6516-7459
Dennis Stello https://orcid.org/0000-0002-4879-3519
Thaisa Storchi-Bergmann https://orcid.org/0000-0003-1772-0023
Guy S. Stringfellow https://orcid.org/0000-0003-1479-3059
Amelia Stutz https://orcid.org/0000-0003-2300-8200
Jing Sun https://orcid.org/0000-0002-8226-2412
Jamie Tayar https://orcid.org/0000-0002-4818-7885
Nicholas W. Troup https://orcid.org/0000-0003-3248-3097
Sarah Tuttle https://orcid.org/0000-0002-7327-565X
Marica Valentini https://orcid.org/0000-0003-0974-4148
Jose Antonio Vázquez-Mata https://orcid.org/0000-0001-8694-1204
David Wake https://orcid.org/0000-0002-6047-1010
Yuting Wang https://orcid.org/0000-0001-7756-8479
W. M. Wood-Vasey https://orcid.org/0000-0001-7113-1233
Renbin Yan https://orcid.org/0000-0003-1025-1711
Gail Zasowski https://orcid.org/0000-0001-6761-9359
Kai Zhang https://orcid.org/0000-0002-9808-3646
Guangtun Zhu https://orcid.org/0000-0002-7574-8078
Hu Zou https://orcid.org/0000-0002-6684-3997

References

Abazajian, K. N., Adelman-McCarthy, J. K., Agüeros, M. A., et al. 2009, ApJS, 182, 543
Abolfathi, B., Aguado, D. S., Aguilar, G., et al. 2018, ApJS, 235, 42
Aguado, D. S., Ahumada, R., Almeida, A., et al. 2019, ApJS, 240, 23
Ahn, C. P., Alexandroff, R., Allende Prieto, C., et al. 2012, ApJS, 203, 21
Aihara, H., Allende Prieto, C., An, D., et al. 2011, ApJS, 193, 29
Alam, S., Albareti, F. D., Allende Prieto, C., et al. 2015, ApJS, 219, 12
Albareti, F. D., Allende Prieto, C., Almeida, A., et al. 2017, ApJS, 233, 25
Allende Prieto, C., Beers, T. C., Wilhelm, R., et al. 2006, ApJ, 636, 804
Anders, F., Khalatyan, A., Chiappini, C., et al. 2019, A&A, 628, A94
Ata, M., Baumgarten, F., Bautista, J., et al. 2018, MNRAS, 473, 4773
Aubourg, É., Bailey, S., Bautista, J. E., et al. 2015, PhRvD, 92, 123516
Bates, D. J., Tojeiro, R., Newman, J. A., et al. 2019, MNRAS, 486, 3059
Bautista, J. E., Busca, N. G., Guy, J., et al. 2017, A&A, 603, A12
Bautista, J. E., Vargas-Magaña, M., Dawson, K. S., et al. 2018, ApJ, 863, 110
Blanton, M. R., Bershady, M. A., Abolfathi, B., et al. 2017, AJ, 154, 28
Blanton, M. R., Kazin, E., Muna, D., Weaver, B. A., & Price-Whelan, A. 2011, AJ, 142, 31
Blomqvist, M., du Mas des Bourboux, H., Busca, N. G., et al. 2019, A&A, 629, A86
Boller, T., Freyberg, M. J., Trümper, J., et al. 2016, A&A, 588, A103
Bolton, A. S., Burles, S., Koopmans, L. V. E., Treu, T., & Moustakas, L. A. 2006, ApJ, 638, 703
Bolton, A. S., Schlegel, D. J., Aubourg, É., et al. 2012, AJ, 144, 144
Bovy, J. 2015, ApJS, 216, 29
Bovy, J., Leung, H. W., Hunt, J. A. S., et al. 2019, MNRAS, 490, 4740
Bovy, J., Nidever, D. L., Rix, H.-W., et al. 2014, ApJ, 790, 127
Brimioulle, F., Seitz, S., Lerchster, M., Bender, R., & Snigula, J. 2013, MNRAS, 432, 1046
Brinchmann, J., Charlot, S., White, S. D. M., et al. 2004, MNRAS, 351, 1151
Brownstein, J. R., Bolton, A. S., Schlegel, D. J., et al. 2012, ApJ, 744, 41
Bundy, K., Bershady, M. A., Law, D. R., et al. 2015, ApJ, 798, 7

Castelli, F., & Kurucz, R. L. 2003, in IAU Symp. 210, Modelling of Stellar Atmospheres, ed. N. Piskunov, W. W. Weiss, & D. F. Gray (Cambridge: Cambridge Univ. Press), A20
Castorina, E., Hand, N., Seljak, U., et al. 2019, JCAP, 09, 010
Chabanier, S., Palanque-Delabrouille, N., Yèche, C., et al. 2019, JCAP, 07, 017
Chabrier, G. 2003, PASP, 115, 763
Cherinka, B., Andrews, B. H., Sánchez-Gallego, J., et al. 2019, AJ, 158, 74
Clerc, N., Kirkpatrick, C. C., Finoguenov, A., et al. 2020, MNRAS, submitted
Clerc, N., Merloni, A., Zhang, Y. Y., et al. 2016, MNRAS, 463, 4490
Clerc, N., Sadibekova, T., Pierre, M., et al. 2012, MNRAS, 423, 3561
Coffey, D., Salvato, M., Merloni, A., et al. 2019, A&A, 625, A123
Comparat, J., Maraston, C., Goddard, D., et al. 2017, arXiv:1711.06575
Comparat, J., Merloni, A., Dwelly, T., et al. 2020, A&A, 636, A97
Cunha, K., Smith, V. V., Hasselquist, S., et al. 2017, ApJ, 844, 145
Cutri, R. M., Wright, E. L., Conrow, T., et al. 2013, in Explanatory Supplement to the AllWISE Data Release Products, ed. R. M. Cutri et al. (Pasadena, CA: IPAC/Caltech), 1
Dawson, K. S., Kneib, J.-P., Percival, W. J., et al. 2016, AJ, 151, 44
Dawson, K. S., Schlegel, D. J., Ahn, C. P., et al. 2013, AJ, 145, 10
de Sainte Agathe, V., Balland, C., du Mas des Bourboux, H., et al. 2019, A&A, 629, A85
Denney, K. D., Horne, K., Brandt, W. N., et al. 2016a, ApJ, 833, 33
Denney, K. D., Horne, K., Shen, Y., et al. 2016b, ApJS, 224, 14
Dexter, J., Xin, S., Shen, Y., et al. 2019, ApJ, 885, 44
Dey, A., Schlegel, D. J., Lang, D., et al. 2019, AJ, 157, 168
Donor, J., Frinchaboy, P. M., Cunha, K., et al. 2018, AJ, 156, 142
Donor, J., Frinchaboy, P. M., Cunha, K., et al. 2020, AJ, 159, 199
Drory, N., MacDonald, N., Bershady, M. A., et al. 2015, AJ, 149, 77
du Mas des Bourboux, H., le Goff, J.-M., Blomqvist, M., et al. 2017, A&A, 608, A130
Dwelly, T., Salvato, M., Merloni, A., et al. 2017, MNRAS, 469, 1065
Eisenstein, D. J., Annis, J., Gunn, J. E., et al. 2001, AJ, 122, 2267
Eisenstein, D. J., Weinberg, D. H., Agol, E., et al. 2011, AJ, 142, 72
Eisenstein, D. J., Zehavi, I., Hogg, D. W., et al. 2005, ApJ, 633, 560
Erfanianfar, G., Finoguenov, A., Furnell, K., et al. 2019, A&A, 631, A175
Falcón-Barroso, J., Sánchez-Blázquez, P., Vazdekis, A., et al. 2011, A&A, 532, A95
Finoguenov, A., Merloni, A., Comparat, J., et al. 2019, Msngr, 175, 39
Finoguenov, A., Rykoff, E., Clerc, N., et al. 2020, A&A, in press
Flaugher, B., Diehl, H. T., Honscheid, K., et al. 2015, AJ, 150, 150
Flewelling, H. A., Magnier, E. A., Chambers, K. C., et al. 2016, arXiv:1612.05243
Furnell, K. E., Collins, C. A., Kelvin, L. S., et al. 2018, MNRAS, 478, 4952
Gaia Collaboration, Brown, A. G. A., Vallenari, A., et al. 2018, A&A, 616, A1
García Pérez, A. E., Allende Prieto, C., Holtzman, J. A., et al. 2016, AJ, 151, 144
Gil-Marín, H., Guy, J., Zarrouk, P., et al. 2018, MNRAS, 477, 1604
Goddard, D., Thomas, D., Maraston, C., et al. 2017a, MNRAS, 466, 4731
Goddard, D., Thomas, D., Maraston, C., et al. 2017b, MNRAS, 465, 688
Grier, C. J., Hall, P. B., Brandt, W. N., et al. 2015, ApJ, 806, 111
Grier, C. J., Shen, Y., Horne, K., et al. 2019, ApJ, 887, 38
Grier, C. J., Trump, J. R., Shen, Y., et al. 2017, ApJ, 851, 21
Gunn, J. E., Siegmund, W. A., Mannery, E. J., et al. 2006, AJ, 131, 2332
Gustafsson, B., Edvardsson, B., Eriksson, K., et al. 2008, A&A, 486, 951
Hemler, Z. S., Grier, C. J., Brandt, W. N., et al. 2019, ApJ, 872, 21
Holtzman, J. A., Hasselquist, S., Shetrone, M., et al. 2018, AJ, 156, 125
Homayouni, Y., Trump, J. R., Grier, C. J., et al. 2019, ApJ, 880, 126
Hunter, J. D. 2007, CSE, 9, 90
Jansen, F., Lumb, D., Altieri, B., et al. 2001, A&A, 365, L1
Jönsson, H., Holtzman, J. A., Allende Prieto, C., et al. 2020, AJ, submitted
Kaiser, N., Burgett, W., Chambers, K., et al. 2010, Proc. SPIE, 7733, 77330E
Kollmeier, J. A., Zasowski, G., Rix, H.-W., et al. 2017, arXiv:1711.03234
Law, D. R., Cherinka, B., Yan, R., et al. 2016, AJ, 152, 83
Law, D. R., Yan, R., Bershady, M. A., et al. 2015, AJ, 150, 19
Leung, H. W., & Bovy, J. 2019a, MNRAS, 483, 3255
Leung, H. W., & Bovy, J. 2019b, MNRAS, 489, 2079
Li, J., Shen, Y., Brandt, W. N., et al. 2019, ApJ, 884, 119
Li, J., Shen, Y., Horne, K., et al. 2017, ApJ, 846, 79
Li, N., & Thakar, A. R. 2008, CSE, 10, 18
Lyke, B. W., Higley, A. N., McLane, J. N., et al. 2020, ApJS, submitted
Mackereth, J. T., & Bovy, J. 2018, PASP, 130, 114501
Mackereth, J. T., Bovy, J., Leung, H. W., et al. 2019, MNRAS, 489, 176
MacLeod, C. L., Green, P. J., Anderson, S. F., et al. 2018, AJ, 155, 6
Majewski, S. R., Schiavon, R. P., Frinchaboy, P. M., et al. 2017, AJ, 154, 94
Maraston, C., & Strömbäck, G. 2011, MNRAS, 418, 2785
Martini, P., Bailey, S., Besuner, R. W., et al. 2018, Proc. SPIE, 10702, 107021F
Matsuoka, Y., Strauss, M. A., Shen, Y., et al. 2015, ApJ, 811, 91
Merloni, A., Alexander, D. A., Banerji, M., et al. 2019, Msngr, 175, 42
Merloni, A., Predehl, P., Becker, W., et al. 2012, arXiv:1209.3114
Morganson, E., Green, P. J., Anderson, S. F., et al. 2015, ApJ, 806, 244
Myers, A. D., Palanque-Delabrouille, N., Prakash, A., et al. 2015, ApJS, 221, 27
Nidever, D. L., Holtzman, J. A., Allende Prieto, C., et al. 2015, AJ, 150, 173
Pace, Z. J., Tremonti, C., Chen, Y., et al. 2019a, ApJ, 883, 82
Pace, Z. J., Tremonti, C., Chen, Y., et al. 2019b, ApJ, 883, 83
Pawlik, M. M., Wild, V., Walcher, C. J., et al. 2016, MNRAS, 456, 3032
Pérez, F., & Granger, B. E. 2007, CSE, 9, 21
Plez, B. 2012, Turbospectrum: Code for Spectral Synthesis v15.1, Astrophysics Source Code Library, ascl:1205.004
Prakash, A., Licquia, T. C., Newman, J. A., et al. 2016, ApJS, 224, 34
Predehl, P., Andritschke, R., Babyshkin, V., et al. 2016, Proc. SPIE, 9905, 99051K
Predehl, P., Andritschke, R., Becker, W., et al. 2014, Proc. SPIE, 9144, 91441T
Price-Whelan, A. M., Hogg, D. W., Foreman-Mackey, D., & Rix, H.-W. 2017, ApJ, 837, 20
Price-Whelan, A. M., Hogg, D. W., Rix, H.-W., et al. 2018, AJ, 156, 18
Price-Whelan, A. M., Hogg, D. W., Rix, H.-W., et al. 2020, ApJ, 895, 2
Prugniel, P., Soubiran, C., Koleva, M., & le Borgne, D. 2007, arXiv:astro-ph/0703658
Queiroz, A. B. A., Anders, F., Chiappini, C., et al. 2020, A&A, 683, A76
Queiroz, A. B. A., Anders, F., Santiago, B. X., et al. 2018, MNRAS, 476, 2556
Raichoor, A., Comparat, J., Delubac, T., et al. 2017, MNRAS, 471, 3955
Reid, B., Ho, S., Padmanabhan, N., et al. 2016, MNRAS, 455, 1553
Robitaille, T. P., Tollerud, E. J., Greenfield, P., et al. 2013, A&A, 588, A33
Robotham, A. S. G., Norberg, P., Driver, S. P., et al. 2011, MNRAS, 416, 2640
Roulston, B. R., Green, P. J., Ruan, J. J., et al. 2019, ApJ, 877, 44
Ruan, J. J., Anderson, S. F., Green, P. J., et al. 2016, ApJ, 825, 137
Rykoff, E. S., Koester, B. P., Rozo, E., et al. 2012, ApJ, 746, 178
Rykoff, E. S., Rozo, E., Busha, M. T., et al. 2014, ApJ, 785, 104
Salvato, M., Buchner, J., Budavári, T., et al. 2018, MNRAS, 473, 4937
Sánchez-Blázquez, P., Peletier, R. F., Jiménez-Vicente, J., et al. 2006, MNRAS, 371, 703
Saxton, R. D., Read, A. M., Esquej, P., et al. 2008, A&A, 480, 611
Shan, H. Y., Kneib, J.-P., Comparat, J., et al. 2014, MNRAS, 442, 2534
Shen, Y., Brandt, W. N., Dawson, K. S., et al. 2015a, ApJS, 216, 4
Shen, Y., Brandt, W. N., Richards, G. T., et al. 2016a, ApJ, 831, 7
Shen, Y., Greene, J. E., Ho, L. C., et al. 2015b, ApJ, 805, 96
Shen, Y., Grier, C. J., Horne, K., et al. 2019a, ApJL, 883, L14
Shen, Y., Hall, P. B., Horne, K., et al. 2019b, ApJS, 241, 34
Shen, Y., Horne, K., Grier, C. J., et al. 2016b, ApJ, 818, 30
Smee, S. A., Gunn, J. E., Uomoto, A., et al. 2013, AJ, 146, 32
Ivezić, Ž, Smith, J. A., Miknaitis, G., et al. 2007, AJ, 134, 973
Stoughton, C., Lupton, R. H., Bernardi, M., et al. 2002, AJ, 123, 485
Sun, M., Trump, J. R., Shen, Y., et al. 2015, ApJ, 811, 42
Sun, M., Xue, Y., Richards, G. T., et al. 2018, ApJ, 854, 128
Talbot, M. S., Brownstein, J. R., Bolton, A. S., et al. 2018, MNRAS, 477, 195
Taylor, M. B. 2005, in ASP Conf. Ser. 347, Astronomical Data Analysis Software and Systems XIV, ed. P. Shopbell, M. Britton, & R. Ebert (San Francisco, CA: ASP), 29
Thakar, A. R., Szalay, A., Fekete, G., & Gray, J. 2008, CSE, 10, 30
Virtanen, P., Gommers, R., Oliphant, T., et al. 2020, Nature Methods, in press
Voges, W., Aschenbach, B., Boller, T., et al. 1999, A&A, 349, 389
Voges, W., Aschenbach, B., Boller, T., et al. 2000, IAUC, 7432, 3
Wake, D. A., Bundy, K., Diamond-Stanic, A. M., et al. 2017, AJ, 154, 86
Walt, S., v. d. , Colbert, S. C., & Varoquaux, G. 2011, CSE, 13, 22
Wang, S., Shen, Y., Jiang, L., et al. 2019, ApJ, 882, 4
Wilkinson, D. M., Maraston, C., Goddard, D., Thomas, D., & Parikh, T. 2017, MNRAS, 472, 4297
Wilkinson, D. M., Maraston, C., Thomas, D., et al. 2015, MNRAS, 449, 328
Wilson, J. C., Hearty, F. R., Skrutskie, M. F., et al. 2019, PASP, 131, 055001
Wright, E. L., Eisenhardt, P. R. M., Mainzer, A. K., et al. 2010, AJ, 140, 1868
Yan, R., Bundy, K., Law, D. R., et al. 2016a, AJ, 152, 197
Yan, R., Chen, Y., Lazarz, D., et al. 2019, ApJ, 883, 175
Yan, R., Tremonti, C., Bershady, M. A., et al. 2016b, AJ, 151, 8
York, D. G., Adelman, J., Anderson, J. E., Jr., et al. 2000, AJ, 120, 1579
Yue, M., Jiang, L., Shen, Y., et al. 2018, ApJ, 863, 21
Zarrouk, P., Burtin, E., Gil-Marín, H., et al. 2018, MNRAS, 477, 1639
Zasowski, G., Cohen, R. E., Chojnowski, S. D., et al. 2017, AJ, 154, 198
Zasowski, G., Johnson, J. A., Frinchaboy, P. M., et al. 2013, AJ, 146, 81
Zhang, K., Schlegel, D. J., Andrews, B. H., et al. 2019, ApJ, 883, 63
Zinn, J. C., Pinsonneault, M. H., Huber, D., & Stello, D. 2019, ApJ, 878, 136